♦ ISEV

RESEARCH ARTICLE

Asymmetric depth-filtration: A versatile and scalable method for high-yield isolation of extracellular vesicles with low contamination

Vasiliy S. Chernyshev[1,2] (ID) | Roman N. Chuprov-Netochin[2] | Ekaterina Tsydenzhapova[2] | Elena V. Svirshchevskaya[3] | Rimma A. Poltavtseva[4] | Anastasiia Merdalimova[1] | Alexey Yashchenok[1] | Amiran Keshelava[5] | Konstantin Sorokin[5] | Varlam Keshelava[6] | Gennadiy T. Sukhikh[4] | Dmitry Gorin[1] | Sergey Leonov[2] | Mikhail Skliar[7,8]

[1]Skolkovo Institute of Science and Technology, Moscow, Russian Federation

[2]School of Biological and Medical Physics, Moscow Institute of Physics and Technology, Dolgoprudny, Moscow Region, Russian Federation

[3]Shemyakin-Ovchinnikov Institute of Bioorganic Chemistry RAS, Moscow, Russian Federation

[4]National Medical Research Center for Obstetrics, Gynecology and Perinatology named after Academician V.I. Kulakov, Ministry of Healthcare of the Russian Federation, Moscow, Russian Federation

[5]Prostagnost LLC, Moscow, Russian Federation

[6]Institute for Biological Instrumentation RAS, Pushchino, Russian Federation

[7]Department of Chemical Engineering, University of Utah, Salt Lake City, UT, USA

[8]The Nano Institute of Utah, University of Utah, Salt Lake City, UT, USA

Correspondence
Vasiliy Chernyshev, Skolkovo Institute of Science and Technology, Moscow, Russian Federation.
Email: v.chernyshev@skoltech.ru

Mikhail Skliar, University of Utah, United State.
Email: mikhail.skliar@utah.edu

Abstract

We developed a novel asymmetric depth filtration (DF) approach to isolate extracellular vesicles (EVs) from biological fluids that outperforms ultracentrifugation and size-exclusion chromatography in purity and yield of isolated EVs. By these metrics, a single-step DF matches or exceeds the performance of multistep protocols with dedicated purification procedures in the isolation of plasma EVs. We demonstrate the selective transit and capture of biological nanoparticles in asymmetric pores by size and elasticity, low surface binding to the filtration medium, and the ability to cleanse EVs held by the filter before their recovery with the reversed flow all contribute to the achieved purity and yield of preparations. We further demonstrate the method's versatility by applying it to isolate EVs from different biofluids (plasma, urine, and cell culture growth medium). The DF workflow is simple, fast, and inexpensive. Only standard laboratory equipment is required for its implementation, making DF suitable for low-resource and point-of-use locations. The method may be used for EV isolation from small biological samples in diagnostic and treatment guidance applications. It can also be scaled up to harvest therapeutic EVs from large volumes of cell culture medium.

KEYWORDS
asymmetric pores, depth filtration, extracellular vesicles, isolation

1 | INTRODUCTION

Isolation of EVs from complex biofluids—such as plasma, urine, saliva, amniotic fluid, and growth medium of cultured cells—is challenging. EV isolations are often contaminated by a complex biomolecular milieu of biofluids, including lipid nanoparticles and protein agglomerates, overlapping with EVs in size and other biophysical properties (Karimi et al., 2018; Sódar et al., 2016; Sun et al., 2019; Zhang et al., 2020). The yield of EVs isolated from such fluids varies significantly by isolation methods. For example, yields between 10^7 and 10^{13} EVs isolated per ml of blood were reported (Arraud et al., 2014; Johnsen et al., 2019; Zhang et al., 2020). In blood and plasma, lipid particles are present at higher concentrations than EVs and contribute considerably to

the contamination even when methods purposefully designed to eliminate them are used. For example, a recently developed elaborate precipitation-purification sequence (Zhang et al., 2020) depletes lipid particles in EV isolations down to an impressive 10%; nevertheless, significant contamination. The contamination by solubilized proteins is similarly variable and was reported to be a microgram of proteins per 10^7 to 10^{11} EVs, depending on the applied isolation method (Buschmann et al., 2018; Jung et al., 2020; Lobb et al., 2015; Martins et al., 2018; Serrano-Pertierra et al., 2019; Webber & Clayton, 2013; Welton et al., 2015).

Most isolation protocols may be assessed by the trade-off they achieve between unbiased high-yield isolation of all EVs present in a biofluid and the purity of isolated EVs. On one extreme, precipitation techniques (Rekker et al., 2014) effectively pull all biological nanoparticles out of biofluid but at the cost of significant contamination by co-precipitated non-EV content. On the other end of the spectrum, immuno-affinity capture (Tauro et al., 2012) isolates the least contaminated EVs but pulls only a minority subpopulation of vesicles that express the capture biomarker (Sidhom et al., 2020). While the sample's purity is essential, biased and fractionated isolations, even when pure, are problematic as they may not adequately represent a multifactorial and multifaceted biological activity of the entire heterogeneous population of EVs (Sidhom et al., 2020; Zhang et al., 2020). Other isolation methods—including ultracentrifugation (Brennan et al., 2020; Chen et al., 2019; Shtam et al., 2018; Taylor and Shah, 2015; Théry et al., 2006; Witwer et al., 2013), size-exclusion chromatography (Baranyai et al., 2015), filtration (Kornilov et al., 2018; Merchant et al., 2010; Nordin et al., 2015), field-flow fractionation (Petersen et al., 2018), and the combinations of methods (Brennan et al., 2020; Nordin et al., 2015; Shtam et al., 2018; Yamada et al., 2012)—may be similarly assessed by their ability to reconcile the difficult task of maximizing the EV yield while minimizing cross contaminations (Liangsupree et al., 2021). Multistep sequences that include dedicated purification procedures are thought to be required to isolate EVs with high yield and purity.

In the following, we introduce asymmetric depth filtration as a novel alternative for unbiased isolation of EVs of high purity using a single-step procedure that only requires a flow reversal across the filtration membrane. Traditional filtration is a widely used separation technique generally divided into surface and depth filtration. Surface filtration strains particles too large to translocate through the filter while solubilized components and small particles pass through the pores. When the sample is flown in the direction normal to the filter's surface (normal-flow filtration), larger particles accumulate on the upstream surface, forming a 'cake' that eventually blocks the pore and impedes further filtration (Sutherland, 2008). Tangential flow filtration (TFF) lessens the cake formation by flowing the sample tangentially to the filter surface, allowing the scale up to higher volumes (Van Reis et al., 1997). In tangential and normal-flow implementations, surface filtration has found applications in the isolation, concentration, and purification of EV preparations (Benedikter et al., 2017; Corso et al., 2017; Haraszti et al., 2018; He et al., 2019; Konoshenko et al., 2018; Kornilov et al., 2018; Le Gall et al., 2020; Lobb et al., 2015; Shu et al., 2020). For example, the isolation of EVs from cell growth medium is possible (Lobb et al., 2015), but we are unaware of successful isolations of EVs by a single-step surface filtration of plasma.

Unlike surface filtration, the depth filtration (DF) medium has pores too large to confine particles entirely on the filter's surface. Instead, particles are fractionated kinetically by the difference in their mobility through the medium. Solubilized components are eluted freely, while the transport of smaller particles is impeded but less than larger ones. Therefore, the carrier flow first elutes small particles. Larger particles are either eluted later or trapped within the depth of the filter. Such trapping may be caused by pores' tortuous geometry, decreasing cross-section in asymmetric filters (Bruil et al., 1991), reduced pores' aperture by the already immobilized particles (Onur et al., 2018; Sutherland, 2008), and interaction with the filtration medium. The accumulation of trapped particles within the filter eventually clogs it. However, since the entire medium participates in fractionation, not just its surface, depth filters can process much larger volumes of biofluid before losing their functionality. Furthermore, the filtering capacity may be entirely or partially regenerated by resuspending and eluting trapped particles by reversing the flow direction (Datta & Redner, 1998; Sutherland, 2008). Additives, such as surfactants and enzymes, may be added to aid the regeneration. Pore sizes and geometry, surface and depth adsorption, and kinetic parameters—such as the flow rate, its duration, and fluid viscosity—may be optimized to efficiently remove impurities by depth filtration. On balance, DF is an adaptable and scalable separation method with broad applications, including large-volume filtrations of wastewater (Darby et al., 1991; Gushing & Lawler, 1998; Salehi et al., 2019) and purification of biomanufactured biologics (Besnard et al., 2016; Bolton et al., 2005; Goldrick et al., 2017; Khanal et al., 2018).

Here we propose asymmetric depth filtration as a universally applicable method for high yield isolation of EVs with low contamination. The developed method immobilizes EVs on the surface and within the depth of porous medium and then recovers them by reversing the carrier flow through the filter. In a single step, it isolates EVs from complex biological fluids, such as plasma, with high yield and purity. We propose mechanisms, and present experimental evidence to support them, which explain the isolation of EVs by asymmetric DF and the contaminant depletion, leading to the reduction in the solubilized background and the number of lipid particles in plasma EV preparations. We demonstrate that the performance of DF in the isolation of plasma EVs (pEVs) compares favourably with the optimized three-step isolation procedure developed by Zhang et al. (Zhang et al., 2020). We quantify the advantages of DF in terms of yield and purity of the isolated pEVs in direct comparison with two established and widely used isolation methods–ultracentrifugation (UC) and size-exclusion chromatography (SEC).

In the current implementation, the developed method will find applications in EV isolations for diagnostic tests and other applications requiring small biofluid volumes, which may be performed at point-of-care and low-resource locations. With a

scale-up to meet biomanufacturing requirements, the method is suitable for isolating therapeutic EVs from large volumes of growth medium used to culture EV-secreting producer cells.

To our knowledge, this is the first report on the isolation of EVs by asymmetric DF.

2 | MATERIALS AND METHODS

2.1 | Participants

Biological samples (blood, urine and Wharton's jelly of umbilical cords) were collected with written informed consent from healthy donors (Protocol № 8 approved on 3 September 2020, by the Institutional Ethical Commission of the FSBI 'National Medical Research Center for Obstetrics, Gynecology and Perinatology named after Academician V.I. Kulakov' of the Ministry of Healthcare of the Russian Federation).

2.2 | Plasma and urine samples

Blood was drawn into EDTA-treated tubes (VACUETTE K2E K2EDTA, Greiner Bio-one, Austria). Cells were removed by centrifugation for 10 min at 1000×g and 4°C. The supernatant was centrifuged again (2000×g and 4°C) to remove platelets and obtain plasma. The collected urine was purified by discarding the pellet precipitated by 30-min centrifugation at 4500×g and 4°C. The samples were aliquoted (1.5 ml of plasma and 15 ml of urine) and stored in Eppendorf tubes (Hamburg, Germany) at −20°C until use.

2.3 | Human multipotent mesenchymal stromal cells (hMMSCs)

The primary MSCs were isolated from the Wharton's jelly of umbilical cords, collected after cesarean section or vaginal births by healthy women who gave prior written informed consent. The isolation of MMSCs followed the previously described protocol (Zhdanova et al., 2021). Briefly, tissue samples were mechanically crushed and placed in 0.1% collagenase Type I solution (Gibco, Thermo Fisher Scientific, Waltham, MA, USA) for 1 h at 37°C. After incubation, the suspension was centrifuged for 3 min at 200×g. Precipitated cells were cultured inside 25 cm^2 culture flasks (Corning, Corning, NY, USA) at 37°C in DMEM/F12 medium (1:1, Gibco) supplemented by 10% fetal calf serum, 2 mM L-glutamine, 100 U/ml of penicillin, and 100 μg/ml of streptomycin (PanEco, Russia). CO$_2$ concertation in the atmosphere was maintained at 5%. Every 72 h, the culture medium was refreshed with 50% of a new medium. When 80% confluence was reached, cells were detached (0.05% trypsin, PanEco), divided (1:2 ratio), and subcultures in 150 cm^2 culture flasks (Corning), each seeded with approximately 5×10^6 cells. After similar division, the third-passage cells were expanded to 80% confluence, washed with 0.9% saline solution, and cultivated in serum-free DMEM/F12 (Thermo Fisher), supplemented with 2 mM of L-glutamine, 100 U/ml of penicillin, and 100 μg/ml of streptomycin medium. After 48 h of incubation, the serum-free medium was collected and used to isolate EVs released by hMMSCs.

2.4 | EV isolation from human plasma, urine, and cell media by depth filtration

The method described here implements asymmetric DF, in which EVs are immobilized on the surface and within the depth of the filter, while small (e.g., lipid) particles, proteins and other solubilized components of plasma, urine and cell culture medium elute with the flow. EVs accumulate inside and on the surface of the filter and are later recovered by reversing the direction of the carrier flow.

We fabricated the DF membrane by dry casting a mixture of cellulose acetates (CA) of different acetyl numbers following a similar approach to the one described by Sossna et al. (2007). The cross-sectional morphology and pore asymmetry of the obtained membrane were characterized by electron microscopy. The SEM image of Surface 1 (Figure 1a) shows entrance apertures of pores wider than EVs. The pores narrow with depth into the membrane (∼20-μm thick) and terminate with much smaller exit apertures seen in the SEM image of Surface 2 (Figure S1). When a sample flows in the forward direction through Surface 1, EVs are retained inside narrowing and tortuous pores (Figure 1b). The immobilized EVs may then be cleansed by the forward flow of a washing buffer to reduce contamination. The reverse flow of resuspending buffer flown in the opposite direction through Surface 2 recovers the immobilized EVs from the membrane for downstream applications.

This study used centrifugal forces to drive forward and reverse flows across the membrane. A disk of DF medium, 22 mm in diameter, was held inside a cylindrical acrylic cartridge (19/25 mm ID/OD) designed to fit inside a standard 50 ml centrifuge tube. Figure 1(c) shows the complete DF assembly (Keshelava et al., 2019). It includes a metal sleeve with a stainless steel mesh
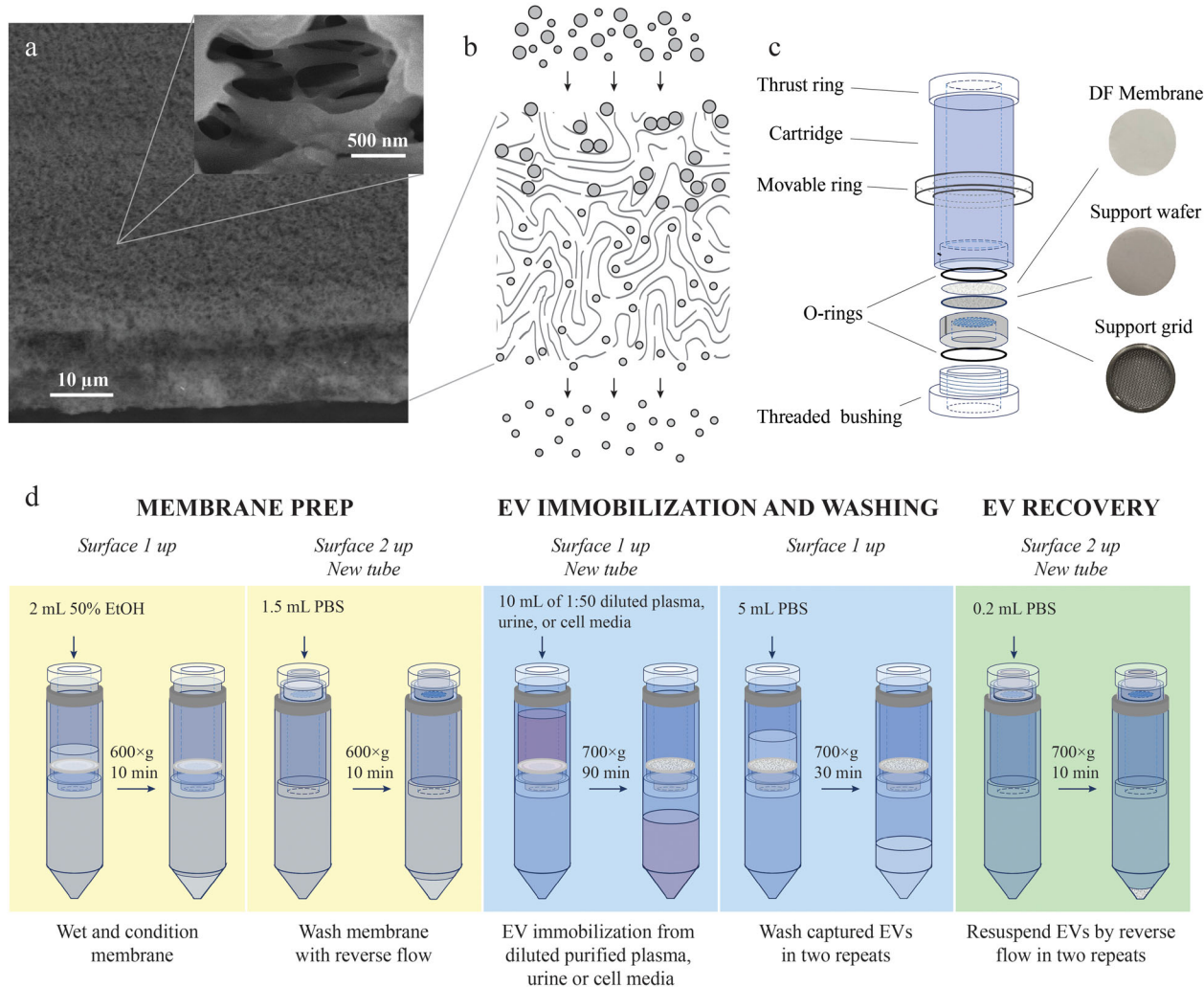
FIGURE 1 Depth-filtration medium, cartridge, and the protocol for DF isolation of EVs from blood plasma, urine, and cell culture media. (a) SEM image of the depth-filtration membrane showing its edge and the entrance surface (Surface 1). Higher magnification (inset) of inlet pores in Surface 1 shows apertures much larger than the size of EVs. As a result, the flow drags vesicles inside the pores until they become immobilized within the depth of the filter. (b) Illustration of the depth filtration process showing two populations of particles of different sizes. Larger particles are retained within the volume of the filtration medium, while smaller particles are eluted. (c) DF cartridge. Photographs of the membrane and its support (porous wafer and stainless-steel grid on which it rests) are shown on the right. (d) Summary of the depth-filtration workflow to isolate EVs from blood plasma, urine, and cell culture media

supporting a porous wafer (Figure S2), which serves as a substrate for the DF membrane. Two silicone O-rings on either side of the membrane cushion the assembly from centrifugal forces, which were kept below 800×g. A threaded plastic bushing is used to securely tighten the membrane between O-rings, thus preventing the fluid from bypassing the membrane during centrifugation. A movable stop ring keeps the assembly inside a centrifuge tube. It slides along the cartridge between the thrust ring and threaded bushing. By manually changing the stop ring's position and reversing the assembly's orientation inside a 50 ml tube, we invert the direction of centrifugal forces and the liquid flow through the DF membrane (EV isolation and washing, forward flow; EV recovery, reverse flow).

Before EV isolation, the filter is wetted and conditioned. 2 ml of 50% ethanol is pipetted onto Surface 1 of the membrane and forced in the forward direction by centrifugation at 600×g for 10 min (Figure 1d) or until all EtOH passes through the filter. This forward flow flushes potential contaminants from a new membrane. Next, the cartridge is flipped to change the membrane orientation, and 1.5 ml of 1 × PBS is pipetted on Surface 2 of the filter inside the small compartment of the cartridge, now facing up (Figure 1d). The buffer is then flown through the filter in the reverse direction to remove residual contaminants and ethanol by centrifuging the assembly for 10 min at 600×g.

EV isolation by DF was performed from 10 ml of biological fluids (diluted plasma and undiluted urine and growth medium). Each sample was loaded on Surface 1 of the depth filter retained inside the DF cartridge, which was inserted into a 50 ml tube (Figure 1d). The flow through the filter was imposed by centrifugation in a swinging bucket rotor at 700×g for 70–90 min or until the sample had passed through the filter. At the completion, the EVs were immobilized within and on the surface of the filter.

Background impurities were removed by washing the immobilized EVs with 5 ml of PBS (washing buffer) flown by centrifugation (700×g for 30 min) in the same direction as the source biofluid (forward flow). This step was repeated for a combined 10 ml of PBS passing through the filter to wash captured EVs.

The immobilized EVs were resuspended by reversing the flow through the DF membrane. A cartridge was flipped to change the filter orientation and inserted into a new 50 ml tube. The resuspending flow was created by centrifuging the assembly for 10 min at 700×g to drive 200 μl of 1 × PBS (resuspending buffer) through the membrane in the reverse direction. This step was repeated to liberate additional EVs trapped inside the filter, giving us the combined ∼400 μl of the preparation containing the isolated EVs for each plasma, urine, and cell culture medium sample. The EV-containing preparation was pipetted several times off and onto the filter to recover EVs remaining on Surface 1, transferred into a 1.5 ml tube (Eppendorf Protein LoBind), and centrifuged for 15 min at 14,000×g to remove bubbles, often introduced by repeated pipetting. Degassed samples were stored at –20°C until further analysis.

2.5 | Isolation of human plasma EVs by ultracentrifugation

Thirty ml of plasma was diluted 1:5 in PBS and aliquoted into five equal volumes. The diluted fluid was transferred into 50 ml tubes and spun at 4500×g at 4°C for 30 min to pellet platelets, residual cells, and debris. The supernatant was transferred to new tubes, and the microvesicles were pelleted by 12,000×g centrifugation for 45 min at 4°C. The supernatant was carefully transferred to 26 ml polycarbonate bottles, and small-size EVs were isolated in two steps by ultracentrifugation using a 70Ti rotor (Beckman Coulter, Brea, CA, USA). First, the samples maintained at 4°C were ultracentrifuged for 70 min at 100,000×g. The supernatant was discarded, and pellets were resuspended in PBS in new 26 ml bottles. The second ultracentrifugation (100,000×g for 70 min) produced EV pellets, which we resuspended in 1 ml of PBS and stored at –20°C in 1.5 ml tubes (Protein LoBind) until analysis.

2.6 | Isolation of human plasma EVs by size-exclusion chromatography

The EV isolation followed the protocol provided by the column manufacturer (PURE-EVs, HansaBioMed, Estonia). The lower Luer cap was removed, and the column was washed with 15 ml PBS flowing at ∼1 ml/min. The lower cap was then reinstalled, and PBS remaining above the column was removed. One ml of thawed plasma maintained at 4°C was centrifuged for 30 min at 4500×g, and 500 μl of obtained supernatant was loaded into the prepared column. The lower cap was removed, and 30-s eluent fractions were collected. As the effluent exited the column, additional PBS was loaded to keep an uninterrupted flow. The flow rate through the column stayed constant at ∼1 ml/min during the procedure, indicating nominal SEC operation. Isolation was repeated five times using different columns. Fractions enriched in EVs were pooled and stored at –20°C.

2.7 | SEM imaging of immunolabelled plasma EVs

The identity of nanoparticles in plasma EV isolations was assessed by the expression of membrane proteins commonly associated with exosomes (CD9, CD63, and EpCAM). First, EVs were labelled with primary antibodies. As-purchased primary Abs (murine anti-CD63, cat. 353013, BioLegend, San Diego, CA, USA; murine anti-CD9, 312102, BioLegend; rabbit anti-EpCAM, ab223582, Abcam, Cambridge, UK) were diluted in PBS containing 0.5% bovine serum albumin (PBS-BSA; pH = 7.2–7.4) to a 1:200 ratio. Dilutions of different Abs were separately mixed with EV samples and incubated for 14 h at 4°C. The incubated samples were further diluted 1:5 in PBS-BSA, and unreacted antibodies were removed by centrifugal filtration (6500×g) through a filter with ∼10-nm pores (Amicon Ultra Centrifugal 100 kDa molecular weight cutoff, MilliporeSigma, Burlington, MA, USA). The Ab-labelled EVs retained by the filter were resuspended for immuno-gold labelling.

The expression of CD9, CD63, and EpCAM on EVs labelled with primary Abs was visualized by SEM using gold nanoparticle reporters binding to Ab-labelled biomarkers. We purchased two types of 20-nm Au nanoparticles, pre-functionalized with secondary mouse or rabbit class G immunoglobulin antibodies (Abcam Goat Anti-Mouse IgG H&L, ab27242; and Goat Anti-Rabbit IgG H&L, ab27237) and designed to react with primary Abs used to label EVs. As-received gold nanoparticles were diluted 1:1000 in PBS-BSA. 50 μl of EV samples labelled by either CD9, CD63, or EpCAM primary antibodies were mixed with 200 μl of diluted AuNPs functionalized with complementary secondary Abs. After incubating the mixture for 6 h at 4°C, unreacted gold nanoparticles were removed by filtration through a 30 nm filter (polycarbonate membrane purchased from Avanti Polar Lipids, Birmingham, AL, USA). EV-AuNP complexes and unreacted EVs retained by the filter were resuspended in 50 μl of deionized water. A small drop of the suspension (∼0.5 μl) was dried at ambient conditions on a clean silicon wafer. The wafer was placed on the specimen stage of SEM (Tescan MAIA3, Brno, Czech Republic), and the desiccated sample was imaged using an accelerating voltage of ∼10.0 kV and magnifications between 100,000 × and 500,000 ×. Gold nanoparticles reported the biomarker expression on the surface of EV membranes as bright spots in the obtained SEM images.

SEM imaging without nano-gold labelling was also performed to visualize the morphology of plasma, urine, and cell culture EVs.

2.8 | Nanoparticle Tracking Analysis (NTA)

Frozen EV samples were thawed and diluted in PBS to concentrations suggested by the manufacturer (Nanosight model NS-300 equipped with 45-mW 488 nm laser; Malvern, Salisbury, UK). Depending on the method used to isolate EVs, the required dilutions were between 1:100 and 1:1000. Within 1 min after the dilution, a sample was injected into the test cell and illuminated by the laser. The light scattered by particles was video recorded for 60 s by a high sensitivity sCMOS camera (camera level set to 14) at 25 frames per second. Each video consisted of 1498 frames. Approximately 30–50 particles were observed in the field of view during video capture, corresponding to concentrations between $\sim 4 \times 10^8$ and 8×10^8 particles per millilitre. The recording was repeated five times for each sample, and the results of their analysis were averaged.

The videos were analysed by Nanosight software (version 3.2) to measure the concentration of EVs, their size distribution, the mode and mean sizes, and the standard deviations of the results. During video analysis, minimum track length, maximum jump mode, and blur size were set to Auto. The detection threshold was 4. The viscosity of PBS was assumed to be that of water at the measured temperature. The NTA instrument automatically measured the sample's temperature, which stayed within 23–24°C throughout the nanoparticle tracking experiments. The water viscosity at this temperature is nearly constant at ~0.91 cP.

2.9 | Dynamic Light Scattering (DLS)

Thawed samples were diluted 1:1000 in PBS, and 1 ml of the preparation was transferred to a low-volume disposable sizing cuvette. After 5-min thermal equilibration inside the DLS instrument (Zetasizer Nano ZS, Malvern Instruments, Malvern, UK), the size distribution and ζ-potential of vesicles were measured at a 173° scattering angle, as recommended by the manufacturer for particles in the 0.3–10,000-nm size range. The sample's viscosity was assumed to be equal to water. The measurements were interpreted by setting the solution's refractive index to 1.33 and 1.35 for EVs (Chernyshev et al., 2015). Samples were analysed in five repeats, each consisting of 12 light scattering measurements. The scattering data were processed assuming a general-purpose model implemented in the Zetasizer software, which estimated EVs' ζ-potential, size distribution, mean, and standard deviations.

2.10 | Western blotting

2.10.1 | EV biomarkers and calnexin

Samples were separated on SDS-PAGE gel (4561103, Bio-Rad, Hercules, CA, USA) and electro-transferred to nitrocellulose membranes (Bio-Rad, 1704158) using Trans-Blot Turbo System (17001917, Bio-Rad). Nonspecific sites were eliminated by washing the membranes with PBS and incubating overnight at 4°C with a blocking buffer (Thermo Fisher, 37572). Primary antibodies for CD9, CD63, EpCAM, Calnexin, Apolipoproteins A1 and B, and UMOD (respectively, BioLegend, 312102 and 353013; LSBio, B6014; Abcam, ab223582; RAH Laa and RAH Lbb, IMTEK, Moscow, Russian Federation; PAG918Hu01, Cloud-clone, Houston, TX, USA) were diluted 1:5000 in blocking buffer and incubated overnight at 4°C with separate membranes inside a gentle shaker. After four 10-min washes with 0.05% PBS-Tween 20 (PBST) solution to remove unreacted antibodies, membranes were incubated at room temperature for 2 h in PBST-0.1% BSA solution of peroxidase-labelled secondary antibodies (P-SAR and P-GAM Iss, IMTEK) diluted 1:5000. The incubated blots were washed (four times with PBST and then again twice with PBS; each wash was 10-min long) and developed using the Clarity Western ECL substrate (Bio-Rad, 170–5060). Precision Plus Protein Western C standard (Bio-Rad, 161-0376) was used for band identification. Immunoreactive bands were visualized with ChemiDoc XRS Imaging System (Bio-Rad, 1708070).

2.10.2 | Human serum albumin

Gel electrophoresis was performed in 10% PAAG using a Bio-Rad electrophoresis system. The transfer of proteins to the Trans-Blot Transfer Media nitrocellulose membrane (Bio-Rad) was carried out using a SemiDry Transfer Cell device (Bio-Rad). The membrane was blocked with 5% milk powder, washed in Tris buffer three times, and stained while shaking for 1 h by mouse anti-human albumin (Hy Test, Moscow, Russian Federation) diluted 1:1000. Human serum albumin (Sigma-Aldrich, St. Louis, MO, USA) was used as a control. The protein ladder standard was provided by a prestained PageRuler Ladder (Thermo Fisher). After incubation, the membrane was washed three times with Tris buffer and incubated for 1 h with anti-mouse antibodies conjugated

with horseradish peroxidase (Santa Cruz Biotechnology, Dallas, TX, USA). After washing the membrane, the proteins were developed with a DAB/NiCl$_2$ solution. The images were acquired using Gel Doc EZ Imager (Bio-Rad).

2.11 | Protein characterization

2.11.1 | UV-Vis absorbance

Protein abundance was quantified using Nanodrop 2000c (Thermo Fisher) following A280 Method. The characterization was performed using 1.5 μl of undiluted samples, repeated four times, and averaged.

2.11.2 | Flow-cytometry

The expression of CD9 and CD63 in all types of examined EV samples—human blood plasma, human urine, and hMMSC culture medium—was established using the Exo-Fluorescence-activated Cell Sorting (FACS) kit (HBM-FACS-C, HansaBioMed). Briefly, EVs were first nonspecifically adsorbed on the surface of large (4-μm diameter) Aldehyde/Sulphate latex beads by co-incubation. Unadsorbed EVs were removed by repeating twice a sequence of bead pelleting by centrifugation, discarding the supernatant, and resuspending the pellet in the fresh buffer supplied with the kit. EVs adsorbed on the beads were then stained for CD9 or CD63 using Abcam ab58989 or ab271286 primary antibodies diluted 1:200 before use. Unreacted Abs were removed by discarding the supernatant after pelleting the labelled bead-EV complexes. A secondary label, reactive with the primary antibodies and conjugated to Alexa Fluor 488 fluorescent dye (ab150113, Abcam), was added after 1:1000 dilution and incubated at 4°C for 1 h with EVs adsorbed on the surface of latex beads and already labelled with primary Abs for CD9 or CD63 biomarkers. Each sample was washed by centrifugation pelleting in the washing buffer (4000×g for 5 min), discarding the supernatant, and refreshing the washing buffer provided with the kit. The prepared samples were analysed by S3 Cell Sorter (BioRad). The data analysis (FlowJo software, BD Life Sciences, Ashland, OR, USA) showed at least 20,000 reads in the FL1 channel for each sample. For confirmation, the results were replicated for each EV sample, and the entire workflow was validated by applying it to plasma EVs supplied with the kit.

As part of the study directly comparing the performance of the asymmetric depth filtration with EV isolation by SEC and UC, the presence of CD81 and reconfirmation of CD9 and CD63 expressions in plasma EVs were performed by screening for epitopes on the surface of exosomes. Briefly, CD9-PE, CD63-APC, and CD81-FITC antibodies (130-103-955, 130-127-492, and 130-107-981; Miltenyi Biotec, Germany) were added to EVs in filtered PEB (PBS plus 5 mM EDTA plus 0.5% BSA), incubated for 60 min at 4°C in a rotator protected from light, and then diluted 1:10 in PEB. MACSQuant Analyzer (Miltenyi Biotec) counted the labelled vesicles. Filtered PEB was run to assess the background noise. Autofluorescence of EVs was evaluated by measuring the unstained EV samples.

2.11.3 | BCA protein analysis

Protein quantification using Micro BCA protein assay (Pierce BCA Protein Assay Kit, Sigma-Aldrich) followed the manufacturer's instructions. In short, EV samples were diluted in DI water (1:1 ratio), and 150 μl of the solution was incubated for 2 h at 35°C with an equal reagent volume. Absorbance was then measured at 562 nm using a ClarioStar plate reader (BMG Labtech, Germany).

2.12 | Raman spectroscopy

The Raman analysis of plasma EVs was performed using a spectrometer (Horiba LabRam Evolution HR, Horiba Ltd., Irvine, CA, USA) equipped with Olympus M Plan 50 × objective and 600 lines/mm grating. Raman scattering was excited by a 633-nm laser adjusted to 50% of its maximum power. A small drop (∼1 μl) of a plasma EV sample was pipetted on a fused quartz surface and dried at room temperature. The analyte concentration was increased by placing the second drop in the exact location and drying. Three spectra were accumulated with a 50-s exposure and averaged. The Raman spectra of the clean area of quartz glass and the dried solution of human serum albumin (0.4 g/ml; Octapharma Pharmazeutika Produktionsgesellschaft m.b.H., Austria) were used as controls.

2.13 | Mass spectrometry and proteomic analysis

2.13.1 | Trypsin hydrolysis

Hydrolytic digestion of proteins was carried out following FASP (Filter-Aided Sample Preparation) protocol (Wiśniewski et al., 2009), which we modified to use 10 kDa NMWCO centrifuge filters (YM-10 Microcon filter, MilliporeSigma). Disulphide protein bonds were restored and alkylated by 30 min incubation with 4 mM Tris (2-carboxyethyl) phosphine (TCEP) and 6.2 mM 2-chloroacetamide (CAA) at 80°C in samples containing 50 μg of protein. The reacted samples were concentrated by using YM-10 centrifuge filters subjected to 11,000×g for 15 min inside a thermostatically controlled rotor maintained at 20°C. Concentrated samples were washed three times by adding 200 ml of buffer containing 50 mM triethylammonium bicarbonate (TEAB, pH = 8.5) and re-concentrated in YM-10 devices (11,000×g for 15 min at 20°C) after each wash. Washed and concentrated samples were suspended in TEAB containing trypsin (Promega, Madison, WI, USA; 1:50 ratio of trypsin to total protein concentration) and incubated overnight at 37°C while shaking at 350 rpm. Peptides were separated from the reaction buffer by 11,000×g thermostatically controlled centrifugation (YM-10 filters) for 15 min, washed with 50 ml of a 30% formic acid, and filtered. The filtrate was dried in a vacuum concentrator and dissolved in 20 μl of 5% formic acid for mass spectroscopy.

2.13.2 | Mass spectrometric (MS) analysis

One microgram of peptide mixture was loaded in Acclaim Pepmap C18 HPLC column (Thermo Fisher) and separated by HPLC in a gradient elution mode (Ultimate 3000 RSLCnano HPLC system, Thermo Fisher). The flow rate of the mobile phase was maintained at 0.3 μl/min. The gradient was formed by mobile phases A (0.1% formic acid) and B (80% acetonitrile, 0.1% aqueous formic acid solution). After washing the column for 7 min (98% and 2% of phases A and B, respectively), the sample was injected, and the concentration of phase B increased linearly to 35% in 63 min and then to 99% in 5 min. The 99% phase B concentration was maintained for 10 min and then linearly decreased to the starting 2% concentration in 5 min.

The mass analysis of the eluted sample was performed by Q Exactive HF-X mass spectrometer (Thermo Fisher) operating with a heated electrospray ionization probe in a positive ionization mode (2.1 kV emitter voltage and 240°C capillary temperature). Panoramic scanning between 300 m/z and 1500 m/z was performed with a resolution set to 120,000. In tandem mass spectrometry mode, the resolution was equal to 15,000 in the mass range between 100 m/z and the upper limit, which was determined automatically based on the mass of the precursor. The isolation of precursor ions was carried out in a ±1 Da window. We set the maximum number of ions isolated in tandem mode to 25, the cutoff limit for selecting a precursor to 80,000 units, and the normalized collision energy NCE = 29. Only ions with charges between z = 2+ and 5+ were considered during tandem scanning. The maximum accumulation time was 50 ms for precursor ions and 100 ms for fragments. The Automatic Gain Control (AGC) value for precursors and fragment ions was set to 1×10^6 and 2×10^5, respectively. All measured precursors were dynamically excluded from tandem MS/MS analysis after 70 s. Protein speciation based on MS measurements was reconstructed in MaxQuant proteomics software (Max-Planck Institute of Biochemistry, Germany), specifying trypsin as the cleavage enzyme and allowing a cleavage site to skip two positions (Walker, 2009). Methionine oxidation and deamidation of glutamine and asparagine were allowed as possible peptide modifications. Carbamoidmethylation of cysteine was assumed to occur. Under the described conditions, the mass of monoisotopic peptides is measured with ±5 ppm accuracy, while the accuracy of masses in MS/MS spectra is equal to ±0.01 Da. The false discovery rate in validating juxtaposition (pair formation) of spectra and peptides was required to be below 1%. At least two peptides were required to validate protein identification.

2.14 | Data analysis

Size-frequency measurements obtained by different techniques were converted into probability density functions (pdf) and visualized as histograms or distributions.

3 | RESULTS

3.1 | EV isolation by asymmetric depth filtration

The asymmetric DF process is illustrated in Figure 1. The opening pores in Surface 1 (Figure 1a) through which the biofluid enters the filtration medium have wider apertures than the diameters of EVs we need to capture and exclude from elution. Therefore, EVs can enter and move through the pores. The EVs' translocation is kinetically controlled by their size, concentration,
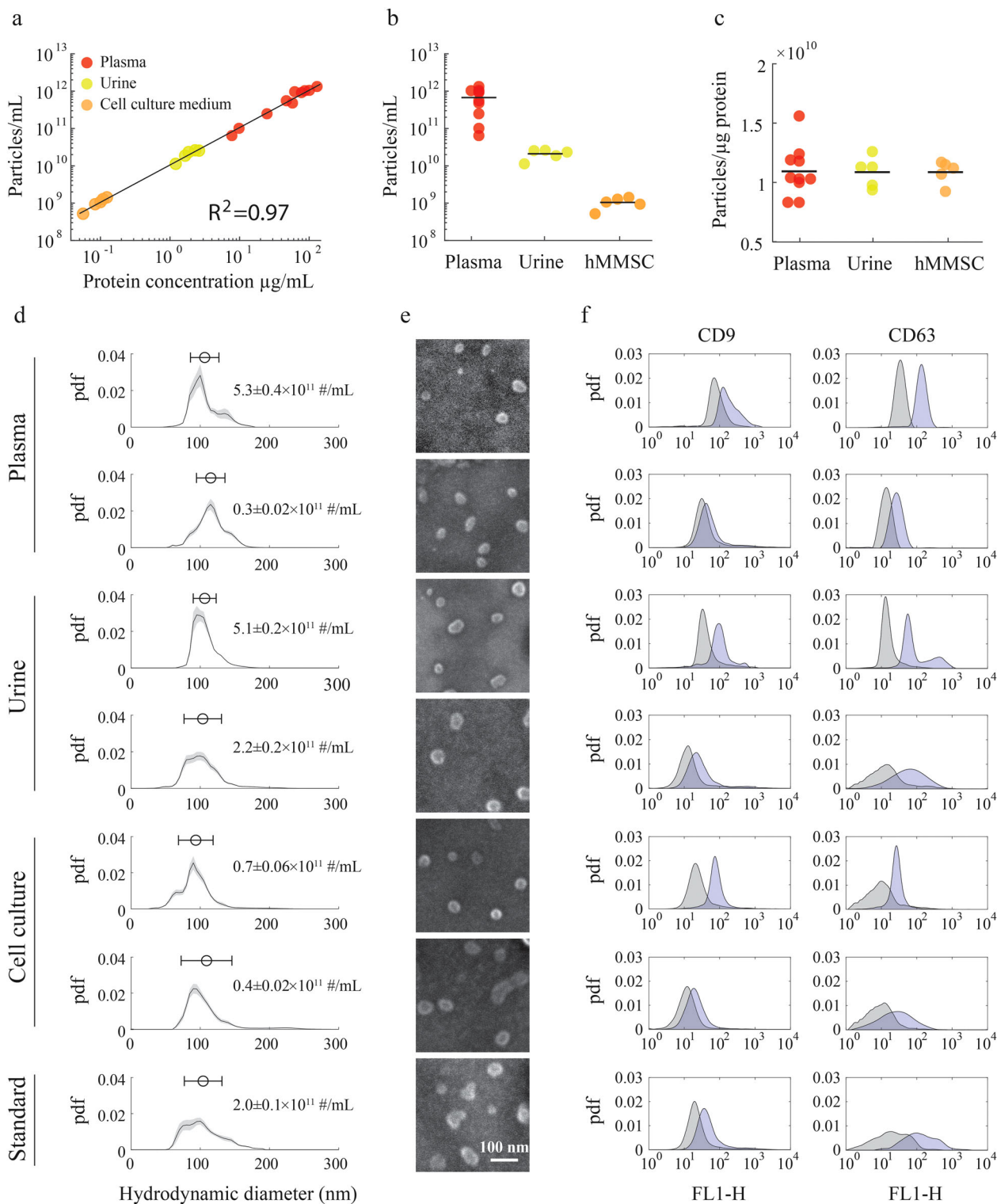
FIGURE 2 Characterization of EVs isolated from plasma, urine, and cell culture media by depth filtration. (a) The number of EVs versus protein concentration in undiluted source biofluids. The slope of the fitted curve is 1.05×10^{10} particles/ml per μg protein. (b) The number of plasma EVs isolated by depth filtration was substantially higher than in the urine. The concentration of EVs in the growth medium was much lower than in body fluids. (c) The number of EVs isolated by DF per μg of proteins in plasma ($n = 10$), urine ($n = 5$), and media of multipotent mesenchymal stromal cells obtained from Warton jelly ($n = 5$). Greater numbers indicate a higher purity of the isolation. The depth filtration consistently produced EV isolation with low protein contamination for all biofluids and biological repeats. (d) Hydrodynamic diameters of isolated EVs in two randomly chosen samples of each biofluid and the purchased EV standard. The size distributions are shown as empirical probability density functions (pdf). The mean $\pm$ standard deviation for each distribution is shown as a circle crossed by a horizontal bar. Each distribution plot lists EV concentration for that sample (#/ml $\pm$ standard error). Each row of results in panels (d)-(e) corresponds to the same sample. (e) SEM images of EVs. (f) Fluorescence-activated cell sorting shows positive CD9 and CD63 biomarkers expression in all EV isolations. Gray-coloured distributions in FACS plots are controls obtained when primary antibodies were not added to the samples. FACS counts were normalized to express the results in pdf form. At least 20,000 events were read in the FL1 channel for every sample
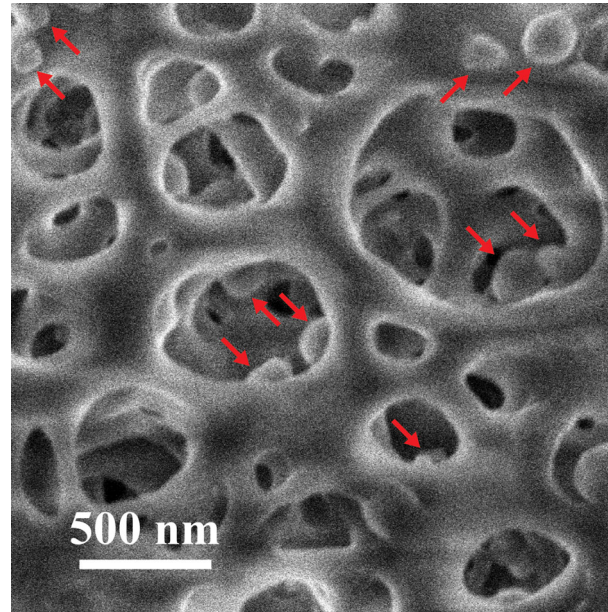
FIGURE 3 SEM image of DF membrane after isolating previously purified plasma EVs. Red arrows indicate vesicles inside the pores and on Surface 1 of the membrane

interactions with pore surfaces, changing pore geometry, and fluid viscosity. Tortoise and narrowing pores of the asymmetric filter (Figures 1a, S1, and schematic in Figure 1b) trap larger particles within the filtration medium while allowing small particles to exit the membrane.

We isolated EVs by DF from biological fluids with widely varying properties. Blood plasma is more viscous and abundant in EVs and proteins than urine (Figures 2a and b). EV and protein concentrations in the growth medium of human multipotent mesenchymal (hMM) stem cells—the third examined biofluid—were significantly lower than either in plasma or urine. Therefore, we adjusted the sample preparation of plasma samples to account for their higher EV and protein concentrations and viscosity. Each blood plasma sample ($n = 10$, 200 μl per donor) was thawed, diluted 1:50 with PBS, and centrifuged at 4500×g for 30 min at 4°C to remove any remaining cell debris and aggregates. The supernatant was cleared by filtration through a 0.8 μm-pore CA filter (Nalgene syringe filter, Thermo Fisher) and transferred into the DF cartridge. The EV isolation from one of the plasma samples was performed in five technical replications to confirm repeatability.

Urine samples from each donor ($n = 5$, 10 ml each) were centrifuged without dilution at 4500×g for 30 min at 4°C. The supernatant was transferred into the DF cartridge without 0.8-μm prefiltration, and EVs were isolated from each sample.

The undiluted culture medium ($\sim$40 ml) was centrifuged for 10 min at 200×g to remove the remaining MMSC cells and another 30 min at 4500×g to remove cell debris. The cleared medium was then filtered through a 0.2 μm filter and transferred for EV isolation by depth filtration. The process was repeated for five media samples obtained after separately culturing MMSCs collected from umbilical cords of five donors ($n = 5$).

The abundance of vesicles relative to the protein concentration characterizes the purity of EV isolations. By this metric, the depth filtration isolated EVs with consistently high purity for all examined biofluid types, on average equal to $\sim$1.1 $\pm$ 0.2 $\times$ 10^{10} vesicles per microgram of proteins (Figure 2c).

Hydrodynamic diameters of the isolated EVs were predominantly in the exosomal/small EVs range (see the size distributions for a subset of samples in Figure 2d and the complete summary of NTA sizing results in Table S1). The electron microscopy examination of EVs isolated from different biofluid types (SEM images of two different samples for each biofluid in Figure 2e) revealed the expected size and morphology of the DF-isolated vesicles. Similar EV size and morphology were observed directly on Surface 1 and inside the pores of the DF membrane (Figure 3 and S3) for plasma EVs, which we purchased as a positive control from HansaBioMed (supplied in purified and lyophilized form, which we suspended in a buffer following manufacturer's instructions) and recaptured by DF.

FACS results in Figure 2(f) show the positive expressions of two canonical EV biomarkers, CD9 and CD63, for the EVs in all biofluids. The biological variability is apparent when comparing EV concentrations and biomarker expressions in samples of the same biofluid type. In each case, the FACS counts positively correlate with EV concentrations. For instance, weak CD63 expression in the second plasma sample, independently confirmed by immunoblotting (Figure B5), is commensurate with lower EV abundance (0.3±0.02 $\times$ 10^{11} #/ml in the second sample *vs.* 5.3±0.4 $\times$ 10^{11} #/ml in the first; Figure 2d). Beyond variations in

the concentration, EVs exhibit molecular heterogeneity, apparent from the binding of immunogold labels to a subset of vesicles (Figure 5e). Such biological heterogeneity likely contributes to the observed differences between the samples.

HPLC-MS proteomic analysis of DF-isolated plasma EVs was performed in three technical repeats for one pEV sample, and 165 proteins were identified in the preparation (SI spreadsheet). The expression of the twenty most abundant proteins is shown in Figure 4(a). The top twenty EV-specific proteins and the parent cells that express them are listed in Table 1. The relative protein abundance is reported as the intensity-based absolute quantification (iBAQ) and the relative iBAQ value (riBAQ) normalized by the total protein abundance. The calculated riBAQ is equivalent to the normalized molar intensity (Shin et al., 2013). Both iBAQ and riBAQ values were obtained using the MaxQuant quantitative proteomics software package.

The presence of contaminating lipid particles of high, low, and very low densities (LDL, HDL, and VLDL), known to collectively exceed the number of EVs in plasma by at least five orders of magnitude (Zhang et al., 2020), was assessed by the relative expressions of lipoproteins in DF-isolated EV preparations. The mass spectroscopy identified nine apolipoproteins that bind lipids to form lipoprotein particles (Mahley et al., 1984). Their relative MS intensity is reported in Figure 4(b). The combined contribution of apolipoproteins is only 7.7% of the total protein content, indicating better than $\times 10^6$ enrichment of EVs achieved by depth filtration relative to lipid particles. This estimate was obtained assuming a linear relationship between the protein concentration and the number of extracellular particles (Figure 2a; also observed by others (Zhang et al., 2020)).

Another common contaminant of plasma EVs is serum albumin, the most abundant protein in the blood. riBAQ data indicates a 7.2% contribution of albumin to the total amount of proteins in EV preparations obtained by DF.

Immunoblotting confirmed the high purity of DF isolations quantified by mass spectroscopy. Western blots of three distinct plasma EV isolations (pEV1...3, Figure 4c) show an essentially complete clearance of apolipoproteins A1 and B by depth filtration compared to their initial expression in source plasma (P1...3).

Unlike plasma, the urine of healthy individuals contains minimal amounts of lipids (Khan et al., 2002). Therefore, we assessed the purity of uEV preparations isolated by DF by the presence of Uromodulin (UMOD), the most abundant urine protein (Tamm & Horsfall, 1950). The Western blot for three isolations of urinary EVs (uEV1...3, Figure 4d) shows thorough depletion of UMOD, expressed abundantly in the source biofluid (U1...3).
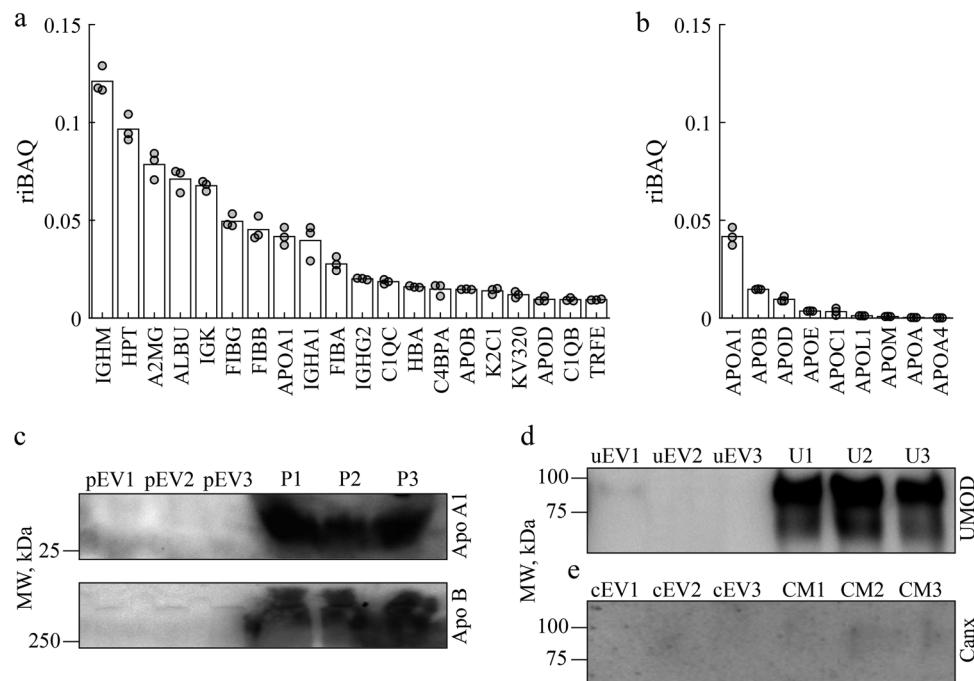

FIGURE 4 Purity of EVs isolated by depth filtration from different biofluids is characterized by the expression of proteins in preparations. (a) Mass spectroscopy determined the twenty most abundant proteins in DF-isolated pEVs quantified by average relative iBAQ values. The complete list of 165 identified proteins is given in SI. Circles indicate values in three repeated proteomic characterizations of the same pEV sample, P1. (b) Relative abundance of nine apolipoproteins in a pEV preparation by HPLC-MS analysis. (c) The expression of apolipoproteins A1 and B in Western blots of three pEV preparations (pEV1...3) indicates their significant depletion by depth filtration of source plasma of different donors (P1...3). Here, pEV1 is the same preparation characterized by mass spectroscopy in panels (a) and (b). P1 plasma sample was also used to compare DF, UC, and SEC isolation methods in Figure 5. (d) Immunoblotting indicates the highly effective elimination of urinary UMOD from DF isolations of urinary EVs (uEV1...3) obtained from the urine of three different donors (U1...3). FACS analysis of CD9 and CD63 expressions in uEV1 and uEV2 is shown in Figure 2(f). (e) Western blotting results indicate Calnexin was not expressed in EVs (cEV1...3) isolated from cell growth media (CM1...3) used to culture primary human MSCs obtained from Warton jelly of three separate umbilical cords. Figure 2(f) shows CD9 and CD63 expressions in cEV1 and cEV2 samples determined by FACS

TABLE 1 The twenty most abundant proteins in plasma EV were identified by mass spectroscopy

UniProt Accession	UniProt ID	Species	Protein name	Expression	References
P01871	IGHM	HUMAN	Immunoglobulin heavy constant mu	B lymphocytes	(Pienimaeki-Roemer et al., 2015; Gonzalez-Begne et al., 2009; Principe et al., 2013)
P00738	HPT	HUMAN	Haptoglobin	Liver	(Principe et al., 2013; Tutanov et al., 2020; Gonzales et al., 2009)
P01023	A2MG	HUMAN	Alpha-2-macroglobulin	Lung, urinary bladder, gall bladder, liver	(Principe et al., 2013; Stamer et al., 2011; Buschow et al., 2010)
P0DOX7	IGK	HUMAN	Immunoglobulin kappa light chain	B lymphocytes	(Guo et al., 2021)
P02679	FIBG	HUMAN	Fibrinogen gamma chain	Liver	(Principe et al., 2013; Tutanov et al., 2020; Gonzales et al., 2009; Melo et al., 2015)
P02675	FIBB	HUMAN	Fibrinogen beta chain	Liver	(Principe et al., 2013; Suárez et al., 2021)
P01876	IGHA1	HUMAN	Immunoglobulin heavy constant alpha 1	B lymphocytes	(Principe et al., 2013; Buschow et al., 2010)
P02671	FIBA	HUMAN	Fibrinogen alpha chain	Liver	(Principe et al., 2013; Gonzales et al., 2009)
P01859	IGHG2	HUMAN	Immunoglobulin heavy constant gamma 2	B lymphocytes	(Principe et al., 2013)
P02747	C1QC	HUMAN	Complement C1q subcomponent subunit C	Spleen, lymph node, lung	(Cheow et al., 2016)
P69905	HBA	HUMAN	Hemoglobin subunit alpha	Heart, spleen, liver	(Reinhardt et al., 2012; Samuel et al., 2017; Ronquist et al., 2013; Ochieng et al., 2009)
P04003	C4BPA	HUMAN	C4b-binding protein alpha chain	Liver, lung, bone marrow	(Gemoll et al., 2020)
P04264	K2C1	HUMAN	Keratin, type II cytoskeletal 1	Skin	(Gonzalez-Begne et al., 2009; Principe et al., 2013; Van Niel et al., 2001)
P01619	KV320	HUMAN	Immunoglobulin kappa variable 3–20	B lymphocytes	(Gonzalez-Begne et al., 2009; Principe et al., 2013)
P02746	C1QB	HUMAN	Complement C1q subcomponent subunit B	Spleen, lymph node, liver	(Mitaki et al., 2021)
P02787	TRFE	HUMAN	Serotransferrin	Liver, nervous system, heart	(An et al., 2017)

(Continues)

TABLE 1 (Continued)

UniProt Accession	UniProt ID	Species	Protein name	Expression	References
P01024	CO3	HUMAN	Complement C3	Liver, gall bladder	(Principe et al., 2013; Stamer et al., 2011)
B9A064	IGLL5	HUMAN	Immunoglobulin lambda-like polypeptide 5	Heart, blood, bone marrow	(Principe et al., 2013)
P13645	K1C10	HUMAN	Keratin, type I cytoskeletal 10	Skin	(Gonzalez-Begne et al., 2009; Principe et al., 2013; Van Niel et al., 2001)
P02751	FINC	HUMAN	Fibronectin	Placenta, liver, lung	(Principe et al., 2013; Gonzales et al., 2009; Atay et al., 2011)

Apolipoproteins quantified in Figure 4(b) and albumin are excluded. Expression data were compiled from NCBI Gene, GeneCards, and UniProtKB databases.

TABLE 2 Mode, mean, and median hydrodynamic diameters (nm) of plasma EVs (plus-minus standard error, STE) measured by NTA and protein concentration (μg/ml) determined by BCA for five repeated EV isolations by different methods

EV isolation method	NTA			BCA
	Mode $\pm$ STE	Mean $\pm$ STE	Median $\pm$ STE	Mean $\pm$ STE
DF	83$\pm$3	109$\pm$2	95$\pm$2	22.7$\pm$2.3
UC	88$\pm$5	101$\pm$4	91$\pm$2	70.7$\pm$1.3
SEC	77$\pm$3	108$\pm$4	92$\pm$4	9.5$\pm$0.2

The absence of cell debris in EV isolations (cEV1…e3) from the culture medium of hMM stem cells (CM1…3 are the media from three independent growth experiments seeded with cells isolated from different umbilical cords) was confirmed by low Calnexin expression (Figures 4e and B3).

3.2 | Comparison of plasma EV isolations by DF, UC and SEC

We used a human plasma sample P1 in a head-to-head comparison of EV purity and yield obtained by depth filtration, ultracentrifugation, and size-exclusion chromatography.

3.2.1 | Plasma EV isolated by depth filtration

The vesicles' hydrodynamic size distributions in pEV1 preparation were measured by NTA (Figures 5a and S4) and DLS (Figure S5). The mean hydrodynamic diameters of these distributions were 109 $\pm$ 2 nm (Table 2) and 97 $\pm$ 1 nm (Table S2) for the two methods. The surface charge of extracellular vesicles was characterized by their ζ-potential, equal to –12.4 $\pm$ 0.5 mV for the DF isolation and similar for other methods (Table S2). The concentration of EVs isolated by DF varied between 2×10^{11} and 3×10^{11} particles/ml in five aliquots of the same P1 sample (Figure 5b, Table S3).

The morphology and the size of EV membranes were assessed by SEM. Figure 5(e) shows the expected rounded shape of desiccated vesicles (Chernyshev et al., 2015) and the geometric size of membrane bilayer envelopes smaller than their hydrodynamic diameter, as expected (Skliar et al., 2018) (Figure S6). The positive expression of CD9, CD63, and EpCAM biomarkers, revealed in SEM images by immunolabelled gold nanoparticles appearing as bright spots on EV membranes, is seen in Figure 5(e).

The protein concentration measured by the BCA assay was between 21 and 29 μg/ml for the DF isolation in the five experimental repeats (Table 2), which puts the EV-to-proteins ratio, often used to characterize the purity of EV isolations, between 1.1 $\times 10^{10}$ and 1.4×10^{10} vesicles per microgram of proteins for the developed method (Figure 5d). Western blotting (Figure 5f) and flow cytometry (Figure 5g) show that EVs express exosomal biomarkers, CD63, EpCAM, and, to a lesser extent, CD9. The most abundant plasma protein, albumin, was undetectable in blots (Figure 5f), though present at low expression according to a more
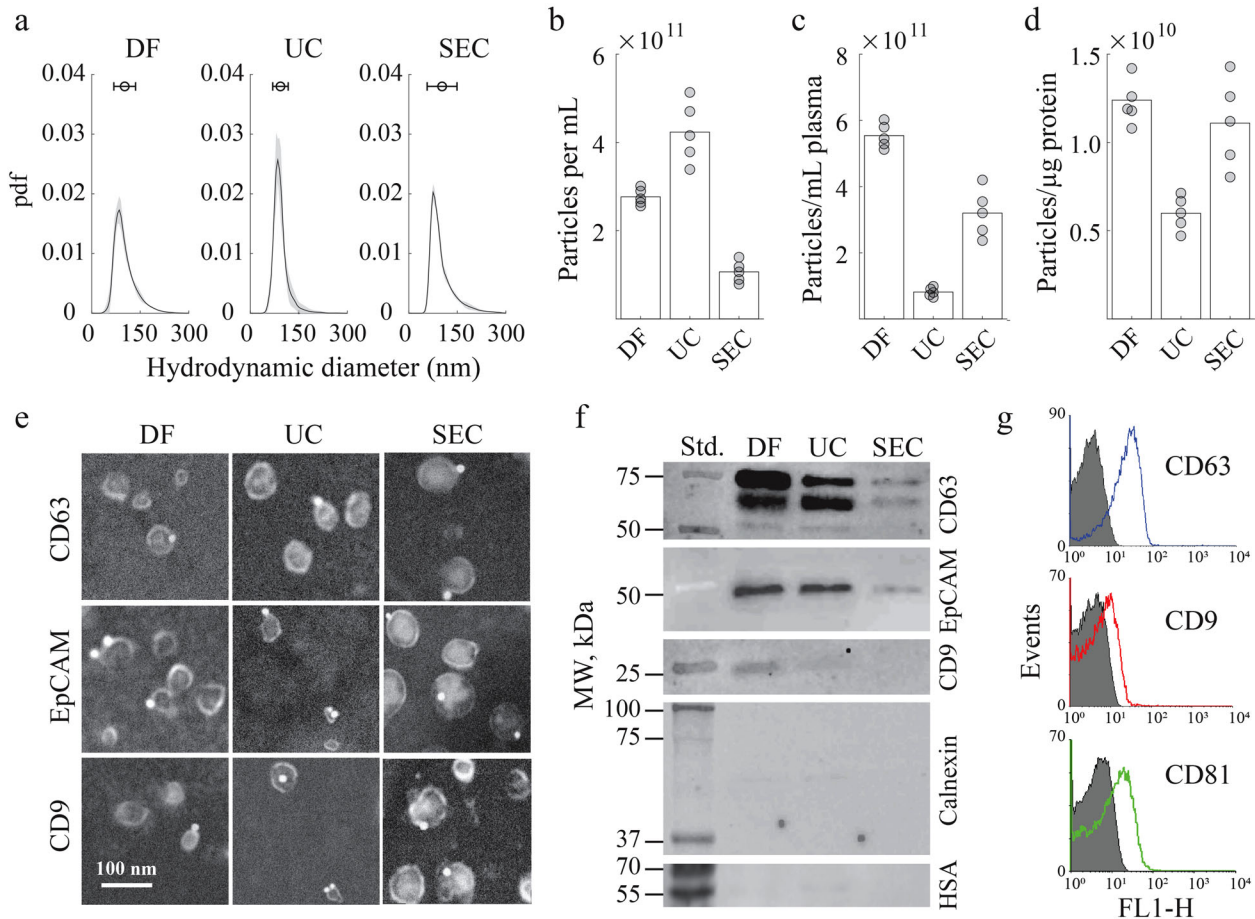
FIGURE 5 Comparison of plasma EVs (five aliquots of P1 sample) isolated by DF, SEC, and UC. (a) The probability density functions show the distribution of hydrodynamic diameters of pEVs isolated by different methods. (b) NTA measurements of EV concentration in different isolations. (c) EVs isolated per ml of plasma. The yield by depth filtration is substantially higher compared to the alternatives. (d) The number of EVs per μg of proteins assesses the purity of EV samples. Co-isolated proteins were at low and comparable levels in DF and SEC preparation and twice as high in UC isolations. (e) SEM images of EVs labelled with CD9, EpCAM, and CD63 primary antibodies. Bright dots on EV membranes are 20-nm gold nanoparticles reporting the locations of biomarker expression. (f) Western blots for EV preparations by different isolation techniques show the highest expression of exosomal biomarkers CD63, EpCAM, and CD9 in the EV sample isolated by DF. The difference in EV concentrations (panel b) contributes to the obtained biomarker expressions. Contaminations evaluated by negative controls (calnexin and human serum albumin) are the lowest in SEC and DF-isolated samples. (g) Flow cytometry analysis shows positive expressions of CD63, CD9, and CD81 biomarkers in DF-isolated EVs

sensitive and quantitative MS/MS (ALBU in Figure 4a). Therefore, we conclude that DF isolation effectively eliminates solubilized plasma proteins from the isolated EVs and significantly depletes lipid particles, as demonstrated by apolipoproteins' low iBAQ values (Figure 4b). Calnexin, an endoplasmic reticulum integral protein, was not expressed in blots (Figure 5f), indicating cell debris does not contaminate DF-isolated EVs.

Raman spectrum of plasma EVs isolated by DF (Figure S7) agrees with previous reports (Krafft et al., 2017; Slyusarenko et al., 2021) and contains the expected peaks identified in Table S4. Specifically, the peak at 1004 cm^{-1} corresponds to aromatic ring stretching in Phenylalanine. The spectral region between 1200 and 1300 cm^{-1} corresponds to amide III bands, and the peak at 832 cm^{-1} is due to out-of-plane ring breathing in Tyrosine. The presence of cholesterol (peak near 704 cm^{-1}) and lipids (peak at 1440 cm^{-1}, corresponding to CH$_2$ bending in lipids and cholesterol) reveals membrane constituents of EVs.

3.2.2 | Isolation by ultracentrifugation

We followed the UC protocol described in references (Filant et al., 2018; Momen-Heravi, 2017). The particle sedimentation by centrifugal forces depends on the particle size, buoyant density, and viscosity of the solution. We reduced the sample's viscosity by diluting plasma with PBS (1:5 ratio) to improve the sedimentation efficiency (Božič et al., 2019; Livshts et al., 2015). We pelleted and discarded any remaining cells, cell debris, apoptotic bodies, large microvesicles, and aggregates by a two-step conventional centrifugation at 4500×g and then at 12,000×g (Momen-Heravi, 2017). The supernatant was then ultracentrifuged at 100,000×g

to pellet EVs. We reduced the background protein contamination by resuspending the pellet in PBS and re-pelleted EVs by the second round of ultracentrifugation at 100,000×g. The second pellet was resuspended in 1 ml of PBS and saved for analysis.

The yield of EVs isolated by UC per ml of plasma was almost an order of magnitude lower than by DF (Figure 5c). The distribution of hydrodynamic sizes (Figure 5a and Table 2) was not significantly different. The ζ-potential was equal to –11.3± 0.8 mV, a comparable value to the electrokinetic potential of DF-isolated vesicles. The EV biomarkers (Figure 5f) were less expressed than in EVs isolated by depth filtration, while the total protein concentration was higher (Table 2). The purity of UC samples, quantified as the number of vesicles per microgram of proteins, was lower than 1×10^{10} particles/μg (Figure 5d). The Western blot in Figure 5(f) indicates the presence of albumin, although, in a low amount, likely contributing to a higher protein concentration (Buzás et al., 2018) in the UC isolation. Albumin was undetectable in Western blots of DF and SEC preparations.

3.2.3 | Isolation by size exclusion

Commercially available SEC columns were used to isolate EVs from 500 μl aliquots of plasma. As the sample flows through a gel-packed column containing porous resin beads, the propagation paths of particles are size-dependent. Proteins, other molecules, aggregates, and small lipid particles migrate through the pores that retard their translocation. Larger particles, such as EVs, cannot enter the pores, migrate through the gel filling the volume unoccupied by beads, and elute first. This fractionation mechanism separates the molecular and particulate content of the sample into fractions eluting at different times.

We collected elution fractions every 30 s, with the first elution interval (Fraction 1, F1) starting at the time when the column is loaded with 500 μl of the plasma sample. We used NTA measurements to determine when to collect EV-containing fractions. We found that particles with hydrodynamic diameters between 90 and 100 nm were predominantly eluted during 30-s intervals 7, 8, and 9 (F7….9, Figure S8). These fractions were pooled and used as the SEC-isolated EV preparation. Fraction 10 contained EVs at a lower abundance relative to protein concentration (less than 1×10^{10} particles/μg of protein) and overlapped with the protein elution time (Figure S8). Later-eluting fractions contained higher protein concentrations (Figure S9) and small particles (mean hydrodynamic diameter between 50 and 60 nm).

EV concentration in pooled fractions F7…9 was between 0.8×10^{11} and 1.4×10^{11} particles/ml (Figure 5b, Table S3), or ~3 times lower than the concentration obtained by DF. Mean hydrodynamic particle diameters measured by DLS (115 ± 9 nm) and NTA (108 ± 4 nm) were consistent with DF and UC isolations. The ζ-potential was –10.8 ± 0.4 mV, close to the values obtained for EVs isolated by alternative methods. Co-isolated proteins in pooled fractions F7-9, measured by BCA protein assay to be 9.5±0.2 μg/ml, were lower in concentration than in UC-isolated samples (Figure 5d). After the normalization with the concentration of the isolated EVs, the abundance of co-isolated proteins was low. On average, a microgram of protein was found in a volume containing $1.1 \times 10^{10} \pm 2.5 \times 10^{9}$ EVs, which is slightly worse than in DF-isolated EVs; however, the variability between the five SEC repetitions with different aliquots was more significant than in very consistent DF isolations, Figure 5(d). Calnexin and albumin (non-EV proteins) were not observed in Western blots for EV preparations isolated by SEC and DF (Figure 5f).

4 | DISCUSSION

EV isolation methods continue to evolve to provide new and improved options to increase the yield and reduce contamination. The maximum possible EV yield is tantamount to unbiased isolation without favouring specific EV subpopulations, which is essential in understanding the impact of biophysical and biochemical heterogeneities on signalling, therapies, and diagnostic applications of EVs. Equally important, the purity of isolations eliminates the potential interference of non-EV components of biofluids on the outcomes.

The goals of isolating EVs from complex biological sources with high yield and low contamination are difficult to achieve simultaneously. Previously proposed solutions usually require multiple processing steps to isolate EVs without bias and then purify the obtained preparation by depleting co-isolated contaminants. For example, a recently proposed three-step isolation sequence (Zhang et al., 2020) starts with high-yield EV precipitation from the source fluid, followed by purification consisting of ultracentrifugation and size exclusion chromatography. The combined sequence is lengthy (requires overnight incubation and 16 h gradient density centrifugation under unusually high forces) and not scalable.

Here, we described a novel asymmetric DF approach to the isolation of EVs from plasma and other biological fluids with yields and purity that exceed multistep methods, such as the one developed by Zhang et al. (2020). The isolation by asymmetric depth filtration is essentially a single-step method that immobilizes EVs from a source biofluid in asymmetric pores, rinses them with washing buffer to deplete contaminants, and then recovers retained EVs by flowing resuspending buffer in the reverse direction.

4.1 | Significance of pore asymmetry

Depth filters typically have uniform pore aperture exceeding the size of impurities they are designed to deplete from the eluting product and may not have a distinct cut-off size. Instead, the separation is kinetic, a feature the DF shares with the SEC. However, proteins, other solubilized components, and smaller particles are eluted first during DF, the opposite of SEC.

Unlike conventional depth filtration, we capture the product (EVs) within the filter, recover it with the reverse flow, and elute impurities into the permeate or permanently immobilize them within the filter. To isolate EVs, we use tortoise and narrowing anisotropic pores (Figures 1a and S1). Such pores stop the motion of EVs entrained by a forward flow of a source biofluid within the filtration medium while allowing solubilized constituents and small biological nanoparticles (e.g., HDL, small LDL, and protein agglomerates in plasma) to exit the membrane (Figure 1b). Reversible protein agglomerates (Narhi et al., 2012), overlapping in size with EVs and retained by the filter, are eliminated by dissociation during wash cycles, aided by high-shear convection of washing buffer inside the pores. Large plasma particles are eliminated from DF isolations during sample preparation (low-speed centrifugation followed by straining larger than $0.8\,\mu$m particles by surface filtration).

LDL and VLDL lipoprotein particles in the range of EV sizes are extremely soft and flexible (Mikl et al., 2011). They deform easily to squeeze into narrowing pores and are forced deep into the asymmetric filter by the forward flow of diluted plasma and eventually either elute as a permeate or lodge permanently within the pores (e.g., become not recoverable after the flow reversal).

Irreversible protein agglomerates with higher than EV elasticity are likely excluded from the DF preparations of pEVs by the same forced elution and trapping mechanisms. Therefore, out of the diversity of protein aggregates in plasma characterized by different sizes, morphology, and structure (Alberti et al., 2010), only those that are irreversible, relatively rigid, and in the range of EV sizes are more likely to contaminate pEV isolations by asymmetric DF. Such isolable stiff protein particles are often associated with diseases (e.g., amyloids in type 2 diabetes (Höppener et al., 2000) and neurodegenerative disorders (Lim et al., 2019)) and should be absent in plasma samples of healthy donors used in this study.

The transit of small lipid particles and solubilized milieu through the depth filter, the forced elution after deformation or trapping of large soft particles (including VLDL and protein agglomerates) within the filtration medium, flushing of residual contaminants from pore surfaces with low protein binding, and dissolving reversible agglomerates during wash cycles are the likely mechanisms behind unprecedented purity of EV isolations obtained by asymmetric depth filtration from plasma, one of the most challenging fluids for isolating EV with high purity.

4.2 | Comparison of asymmetric DF with surface filtration

The pore asymmetry explains the success of the developed DF method in isolating EVs with high purity and yield from complex biofluids when conventional surface filtration fails. In the absence of literature reports on the successful isolation of plasma EVs by a single-step surface filtration, we attempted such isolation ourselves to elucidate the difficulties and highlight the differences with the developed method. Sample preparation steps were the same as for depth filtration. Briefly, plasma was diluted in PBS 1:50, centrifuged at 4500×g for 30 min at 4°C, and the supernatant was filtered through a $0.8\,\mu$m filter. The prepared sample was forced through a 100 kDa MWCO filter (Amicon, MilliporeSigma) by 3500×g centrifugation to isolate EVs. We found that this surface filter clogs quickly, after which continued centrifugation did not reduce the volume of the remaining sample that had not yet passed through the filter, indicating failed isolation.

Conversely, asymmetric pores with entrance apertures larger than EVs maintain flow connectivity, allowing solubilized content and small particles in the plasma to elute even when a significantly lower driving force (700×g) is used.

4.3 | Importance of filter's surface properties

The selection of DF filtration medium contributed to the high yield and purity of EV isolations achieved by the developed method. We chose the CA membrane, known to have one of the lowest protein bindings, partly due to its negative surface charge (Ghaemi et al., 2012). Other biomolecules and particles with a negative ζ-potential at physiological conditions are impeded from nonspecific adsorption to CA. As a result, proteins, small (e.g., lipid) particles, and membrane fragments do not bind to pore surfaces and are easily removed from the filtration medium by the forward flow during EV washing. The negative surface charge of the filtration medium also prevents the adsorption of surface-active EVs (Chernyshev et al., 2022), known to have a negative ζ-potential at neutral acidity, as confirmed in this study. This low affinity of EVs to CA surfaces contributes to their efficient recovery by the reverse flow and the high yield of DF isolations.

Low surface binding enhances the removal of contaminants by washing captured EVs and contributes to the high purity of preparations. Using the same DF device to capture and clean EVs streamlines the isolation workflow.

TABLE 3 Apolipoproteins in EV preparations of Zhang et al. (2020) (three-step protocol) and by depth filtration

	APOB	APOA1	APOA2	APOC3	APOE	APOA4	APOC1	APOA	APOC4	APOD	APOA5	APOL1	APOF	APOM
Three-step protocol	x	x	x	x	x	x	x	x	x	x	x	x	x	x
Depth filtration	x	x			x	x	x	x		x		x		x

Western blots in Figure B1(b) illustrate the decrease in apolipoprotein content of plasma EV preparations with repeated washes. Figure B4(e) shows the reduction in albumin contamination of captured but unwashed pEVs (DF-0) after we subject them to a single (DF-1) and repeated washes (DF-2 lane is for twice and DF-3 for trice-washed EV captures). We found that two washes strike a balance between the purity and EV yield for all examined biofluids (e.g., note the reduction in UMOD expression after the second wash of urine EVs, Figure B2). However, the user has the discretion to perform fewer washes when a higher yield is essential (Figure S3a illustrates that some EVs are lost into permeate with each wash). Alternatively, more than two wash cycles may be performed when a deeper depletion of background contaminants is desired.

4.4 | High purity and yield of EV isolations from different specimen types

We assessed the performance of asymmetric depth filtration by the yield and purity of EVs isolated from three biological fluids–plasma, urine, and cell growth medium. The yield of plasma EVs for ten donor samples (Figure 2a and b), replicated five times for one of the samples (Figure 5c), was between $\sim 6 \times 10^{10}$ and 1×10^{12} vesicles per ml of plasma. We estimate that only $\sim 0.16\%$ of original plasma apolipoprotein A1 and $\sim 0.07\%$ of apolipoprotein B remain in EV preparations, indicating a dramatic depletion of lipid particles by DF. This calculation assumes the reported concentration of apolipoprotein A1 and B in human plasma (1.4 and 1.1 mg/ml, respectively (Vázquez-Oliva et al., 2018)), $\sim 52\ \mu g$/ml total protein concentration in DF-isolated EV preparations measured by BCA (Table 2), and the relative abundance of lipoproteins determined by proteomic analysis (4.23% and 1.50% for APOA1 and APOB, Figure 4b). Similarly, the reduction in albumin from ~ 42 mg/ml in plasma (Vázquez-Oliva et al., 2018) down to 7.22% (riBAQ value) of 52 μg/ml estimates the depletion of the solubilized background by depth filtration down to 0.009% of the original plasma milieu remaining in EV preparations. Apolipoproteins, which quantify contamination by lipid particles, and albumin (the primary solubilized contaminant) contribute similarly to the protein content of isolated pEVs (7.7% and 7.22% riBAQ values, respectively). Semiquantitative immunoblotting analysis (Figures 4c and 5f) is consistent with this MS-based observation.

The analysis of urine EVs and EVs secreted by cultured primary human multipotent MSCs obtained from Warton's jelly show negligible contamination by UMOD and Calnexin, respectively.

Overall, protein contamination was low across all examined biofluids (Figures 4c, d, and e). The ability to isolate EVs with consistently high yield irrespective of sources while depleting the preparations from the most typical contaminants demonstrates the universality of asymmetric depth filtration in isolating extracellular vesicles from biological fluids.

4.5 | Comparison with best-in-class multistep isolations

We compared the purity of DF isolations with that of a three-step isolation-purification sequence of Zhang et al. (2020). The three-step method produced plasma EV preparations containing approximately 10% of lipid particles according to cryo-TEM image analysis. The mass spectroscopy identified 14 distinct apolipoproteins contributing to lipid contamination. Only nine apolipoproteins were present in DF-isolated preparation (Figure 4b, Table 3 and spreadsheet).

Although riBAQ values interpret proteomics data with higher accuracy, these values were not reported in (Zhang et al., 2020), and albumin was not included in the analysis. To obtain a fair comparison, we also excluded albumin (HSA) from calculations and evaluated the percentage of apolipoproteins using MS/MS count rather than riBAQ values. In doing so, we found apolipoproteins in DF samples to comprise 15% of all identified proteins (this value goes down to 14% when HSA was included). This contribution is significantly lower than the 28% reported in (Zhang et al., 2020), which leads us to conclude that a single-step DF method is more efficient at eliminating lipid particles from plasma EV preparation than a lengthy multistep isolation-purification sequence of Zhang et al.

Given $\sim 8 \times 10^{16}$ lipid particles of all types are present in a 1 ml of plasma (Garvey et al., 2003) and conservatively assuming the depth filtration depletes them down to the same 10% contamination as in the three-step protocol (or $\sim 6 \times 10^{10}$ lipid particles per ml based on the average yield of pEVs reported in Figure 2), the developed method depletes lipid particles in EV preparations by at least $\times 10^6$ compared to their abundance in plasma.
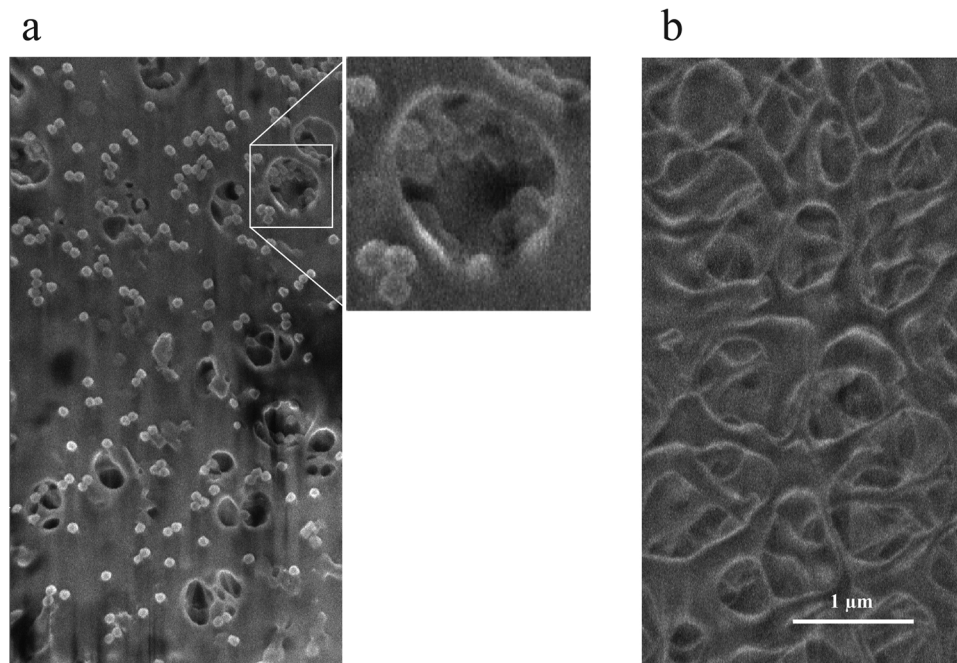
FIGURE 6 (a) SEM image of cellulose acetate DF membrane after the PBS suspension of 100-nm latex beads was flown through it. Beads are visible inside the pores (inset) and on the entry surface of the membrane (Surface 1). (b) Beads were not observed on the exit surface (Surface 2)

4.6 | Comparison with widely used isolation methods

We directly compared the asymmetric depth filtration with two EV isolation methods in wide use, UC and SEC. The EV per ml of human plasma was significantly higher in isolations by depth filtration (Figure 5c), indicating it captures the least biased and the most representative EV population out of examined methods (Buschmann et al., 2018, Rekker et al., 2014, Yang et al., 2021). EV biomarkers (CD63, CD81, CD9, and EpCAM, Figures 5e and f) were most expressed in DF-isolated samples, while the contamination by plasma proteins and membrane debris, respectively, indicated by HSA and Calnexin expressions, was the lowest (Figure 5f).

4.7 | Size selectivity of asymmetric pores

We used two types of synthetic nanoparticles to demonstrate the size selectivity of the depth filter used in this study. The first sample was a suspension of rigid 100-nm NIST-traceable size-standard polystyrene (latex) beads (Polysciences, Inc., Warrington, PA, USA; the size distribution measured by NTA is shown in Figure S10b) diluted in PBS to 1×10^{11} particles/ml. Latex beads have a negative ζ-potential, and the selected size is close to the mean diameter of plasma EVs (Table 2). The suspending buffer, void of a complex molecular milieu of plasma, easily transits the filter. We, therefore, modified the protocol for capturing latex beads from the PBS, as shown in Figure S10(a). Specifically, we used lower forces (400×g) and shorter (7–8 min) centrifugation, which were sufficient to drive the entire 3.75 ml of the sample through the filter.

Figure S10(c) shows that only a small fraction of 100-nm beads (less than 1%) transited through the filter with the permeate. Approximately 88% of particles in the source fluid were recovered after 2 ml of PBS was repeatedly pipetted on and aspirated off the filter (Surface 1). Particles recovered by aspiration were likely retained near pore entrances and on the membrane's top surface. In fact, after flowing the bead suspension through the filter, many particles are visible inside pores and on Surface 1 of the membrane (SEM image in Figure 6a and the inset). No particles were observed on Surface 2 nor inside its exit pores of the filter (Figure 6b). We then reversed the flow direction by changing the orientation of the filter assembly and forcing 2 ml PBS across the membrane by 5-min centrifugation at 400×g in three repetitions. Sequentially, the reverse flow recovered 1.7%, 0.3%, and 0.1% of latex beads in the original sample, Figure S10(c). The remaining ~10% of the particles were permanently lodged within the filter and could not be resuspended.

The second examined synthetic sample was a suspension of 20-nm gold nanoparticles functionalized with anti-mouse IgG (ab27242, Abcam) diluted in PBS to 1×10^{11} particles/ml. These particles have protein-decorated surfaces and were selected to test if smaller-than-EVs particles, such as HDL and small LDL lipoproteins, and solubilized proteins readily pass through the depth filter and do not contaminate EVs recovered by the reverse flow. Indeed, we found that Au particles easily transit through

the filter. Approximately 90% of them eluted with the permeate (Figure S10c). Very few Au particles were recovered by the reverse flow of PBS, which we imposed three times for the total of 6 ml of flowing fluid forced through the filter.

4.8 | Isolation of soft versus rigid nanoparticles

For two types of similarly sized nanoparticles, soft and rigid, we experimentally assessed the impact of particle elasticity on their transit through the asymmetric pores of the depth filter and irreversible trapping within the filtration medium. As soft nanoparticles, we used plasma EVs purchased in purified and lyophilized form from HansaBioMed and rehydrated following the manufacturer's instructions. Latex beads described above were used as rigid nanoparticles.

Figure S3(a) shows a higher number of soft EVs transiting the filter with the flow in the forward direction. Specifically, 16.4±1.6% of vesicles have eluted the filter with the forward flow during EV recapture by DF. Additional 9.7±1.0% and 7.3±0.8% exited into the permeate during the first and the second washes. In contrast, less than 1% of latex beads traversed the filter with the flow in the forward direction. A comparable number of EVs and beads (∼8% and 10%, respectively) were not recovered and were presumably trapped inside the filter. DF captured approximately 90% of latex beads in the original sample compared to ∼60% of plasma EVs. Even with losses, the DF yield of pEVs remains much higher than with widely used isolation methods (Figure 5c).

Several factors likely contributed to a higher percentage of soft EVs eluting through asymmetric pores, while rigid beads did not. First, EVs are size distributed (Figure S3b). Some are smaller than 100-nm monodispersed beads, even though the mean diameter of all EVs is similar. Smaller EVs elute more readily, contributing to a higher loss. Second, the soft coronal layer surrounding the membrane envelope of EVs and contributing to their hydrodynamic diameter can flex to allow the translation through the pores (Skliar et al., 2018). Akin to conformational changes of flexible molecules diffusing through extracellular matrix while rigid molecules of the same size are restricted (Syková & Nicholson, 2008), the flexible corona of EVs may allow their transit through the pore when rigid beads of the same hydrodynamic size are arrested.

The elasticity of EVs' membrane may also play a role in their ability to translocate through asymmetric pores, especially for EVs of larger sizes for which the conformation of the coronal layer alone is insufficient to elute from a pore.

The increasing size of EVs eluted with repeated forward flows (Figure S3b) provides the strongest indication that the compliance of soft nanoparticles to the narrowing geometry of asymmetric pores aids in their transition through asymmetric pores and the elution of ever-larger particles with repeated attempts. The loss of rigid beads into the permeate remains negligible with the number of attempts to elute them (Figure S10c).

LDL and VLDL particles, being softer than EVs, deform more readily and are more likely to elute from the filter or travel deeper into narrowing pores to become permanently trapped.

5 | CONCLUSION, ALTERNATIVE IMPLEMENTATIONS AND APPLICATIONS

The admirable performance of asymmetric depth filtration in isolating EVs may be attributed to the selective transit and capture of biological nanoparticles in asymmetric pores by size and elasticity and the ability to clean the captured EVs in situ before their recovery by the reverse flow. We believe the developed method is the first to utilize the difference in the elasticity of biological nanoparticles to improve the purity of EV preparations. Such selectivity is achieved by a higher propensity of highly compliant particles (e.g., LDL and VLDL) to be forced through asymmetric pores by the forward flow during sample filtration and wash cycles or irreversibly lodge within the pores.

In summary, this report describes a novel approach to EV isolation by asymmetric depth filtration. The developed method is simple and inexpensive. It reproducibly isolates EVs with high yield and purity from complex biological fluids in 3–4 h using only basic laboratory equipment, such as a conventional centrifuge capable of producing 700×g forces. Therefore, it may be used in point-of-care applications and even implemented with manually-powered centrifugation (Bhamla et al., 2017) in field applications and low-resource locations. The main components of the DF cartridge can be reused after cleaning (e.g., soaking in chlorhexidine solution and then rinsing with deionized water), and only the asymmetric DF membrane must be replaced before each isolation. The method may be scaled up by simultaneously processing multiple centrifuge tubes up to the capacity of a rotor. A more significant throughput needed to harvest clinically meaningful quantities of therapeutic EVs from large volumes of growth medium is possible with purpose-designed centrifugation equipment or by using displacement- or pressure-driven flows normal or tangential to DF medium. In diagnostic and other applications where the isolation of EVs from smaller than 5 ml volumes is desirable, the DF cartridge in Figure 1(c), scaled down to be compatible with 500 μl centrifuge tubes, will require only ∼50 μl of a biofluid.

EV-TRACK

AUTHOR CONTRIBUTIONS

Vasiliy S. Chernyshev and Mikhail Skliar conceived the study, designed experiments, interpreted the results, and wrote the manuscript. Vasiliy S. Chernyshev conducted EV isolation, NTA, and SEM analysis. Roman N. Chuprov-Netochin and Ekaterina Tsydenzhapova performed Western blotting and BCA analysis. Elena V. Svirshchevskaya and Rimma A. Poltavtseva performed flow cytometry and Western blotting of human serum albumin. Anastasiia Merdalimova and Alexey Yashchenok performed Raman spectroscopy and peak identification. Amiran Keshelava, Konstantin Sorokin, and Varlam Keshelava contributed to the design and fabrication of the DF cartridge. Gennadiy T. Sukhikh, Sergey Leonov, and Dmitry Gorin provided laboratory equipment and guidance. Vasiliy S. Chernyshev and Mikhail Skliar explained and validated the isolation mechanism and quantified its performance with synthetic particles. Everyone contributed to the manuscript editing.

CONFLICT OF INTERESTS

Aspects of the technology described herein are the subject of a United States provisional patent application.

ORCID

Vasiliy S. Chernyshev ORCID https://orcid.org/0000-0003-2372-7037

REFERENCES

Alberti, S., Halfmann, R., & Lindquist, S. (2010). Biochemical, cell biological, and genetic assays to analyze amyloid and prion aggregation in yeast. *Methods in Enzymology*, *470*, 709–734.

An, M., Lohse, I., Tan, Z., Zhu, J., Wu, J., Kurapati, H., Morgan, M. A., Lawrence, T. S., Cuneo, K. C., & Lubman, D. M. (2017). Quantitative proteomic analysis of serum exosomes from patients with locally advanced pancreatic cancer undergoing chemoradiotherapy. *Journal of Proteome Research*, *16*, 1763–1772.

Arraud, N., Linares, R., Tan, S., Gounou, C., Pasquet, J. - M., Mornet, S., & Brisson, A. R. (2014). Extracellular vesicles from blood plasma: Determination of their morphology, size, phenotype and concentration. *Journal of Thrombosis and Haemostasis*, *12*, 614–627.

Atay, S., Gercel-Taylor, C., Kesimer, M., & Taylor, D. D. (2011). Morphologic and proteomic characterization of exosomes released by cultured extravillous trophoblast cells. *Experimental Cell Research*, *317*, 1192–1202.

Baranyai, T., Herczeg, K., Onódi, Z., Voszka, I., Módos, K., Marton, N., Nagy, G., Mäger, I., Wood, M. J., El Andaloussi, S., Pálinkás, Z., Kumar, V., Nagy, P., Kittel, Á., Buzás, E. I., Ferdinandy, P., & Giricz, Z. (2015). Isolation of exosomes from blood plasma: Qualitative and quantitative comparison of ultracentrifugation and size exclusion chromatography methods. *PLoS One*, *10*, e0145686.

Benedikter, B. J., Bouwman, F. G., Vajen, T., Heinzmann, A. C. A., Grauls, G., Mariman, E. C., Wouters, E. F. M., Savelkoul, P. H., Lopez-Iglesias, C., Koenen, R. R., Rohde, G. G. U., & Stassen, F. R. M. (2017). Ultrafiltration combined with size exclusion chromatography efficiently isolates extracellular vesicles from cell culture media for compositional and functional studies. *Science Reports*, *7*(1), 15297.

Besnard, L., Fabre, V., Fettig, M., Gousseinov, E., Kawakami, Y., Laroudie, N., Scanlan, C., & Pattnaik, P. (2016). Clarification of vaccines: An overview of filter based technology trends and best practices. *Biotechnology Advances*, *34*, 1–13.

Bhamla, M. S., Benson, B., Chai, C., Katsikis, G., Johri, A., & Prakash, M. (2017). Hand-powered ultralow-cost paper centrifuge. *Nature Biomedical Engineering*, *1*, 0009.

Bolton, G. R., Lacasse, D., Lazzara, M. J., & Kuriyel, R. (2005). The fiber-coating model of biopharmaceutical depth filtration. *AIChE Journal*, *51*(11), 2978–2987.

Božič, D., Sitar, S., Junkar, I., Štukelj, R., Pajnič, M., Žagar, E., Kralj-Iglič, V., & Kogej, K. (2019). Viscosity of plasma as a key factor in assessment of extracellular vesicles by light scattering. *Cells*, *8*(9), 1046.

Brennan, K., Martin, K., Fitzgerald, S. P., O'sullivan, J., Wu, Y., Blanco, A., Richardson, C., & Mc Gee, M. M. (2020). A comparison of methods for the isolation and separation of extracellular vesicles from protein and lipid particles in human serum. *Science Reports*, *10*(1), 1039.

Bruil, A., Van Aken, W. G., Beugeling, T., Feijen, J., Steneker, I., Huisman, J. G., & Prins, H. K. (1991). Asymmetric membrane filters for the removal of leukocytes from blood. *Journal of Biomedical Materials Research*, *25*, 1459–1480.

Buschmann, D., Kirchner, B., Hermann, S., Märte, M., Wurmser, C., Brandes, F., Kotschote, S., Bonin, M., Steinlein, O K., Pfaffl, M W., Schelling, G., & Reithmair, M. (2018). Evaluation of serum extracellular vesicle isolation methods for profiling miRNAs by next-generation sequencing. *Journal of Extracellular Vesicles*, *7*, 1481321.

Buschow, S. I., Balkom, B. W. M., Aalberts, M., Heck, A. J. R., Wauben, M., & Stoorvogel, W. (2010). MHC class II-associated proteins in B-cell exosomes and potential functional implications for exosome biogenesis. *Immunology and Cell Biology*, *88*, 851–856.

Buzás, E. I., Tóth, E. Á., Sódar, B. W., & Szabó-Taylor, K. É. (2018). Molecular interactions at the surface of extracellular vesicles. *Seminars in Immunopathology*, *40*, 453–464.

Chen, B.-Y., Sung, C. W.-H., Chen, C., Cheng, C.-M., Lin, D. P.-C., Huang, C.-T., & Hsu, M.-Y. (2019). Advances in exosomes technology. *Clinica Chimica Acta*, *493*, 14–19.

Cheow, E. S. H., Cheng, W. C., Lee, C. N., De Kleijn, D., Sorokin, V., & Sze, S. K. (2016). Plasma-derived extracellular vesicles contain predictive biomarkers and potential therapeutic targets for Myocardial Ischemic (MI) injury. *Molecular & Cellular Proteomics*, *15*, 2628–2640.

Chernyshev, V. S., Chuprov-Netochin, R. N., Tsydenzhapova, E., Van Devener, B., Leonov, S., Gorin, D., & Skliar, M. (2022). Dynamic surface tension probe for measuring the concentration of extracellular vesicles. *Biochemical and Biophysical Research Communications*, *609*, 189–194.

Chernyshev, V. S., Rachamadugu, R., Tseng, Y. H., Belnap, D. M., Jia, Y., Branch, K. J., Butterfield, A. E., Pease, L. F., Bernard, P. S., & Skliar, M. (2015). Size and shape characterization of hydrated and desiccated exosomes. *Analytical and Bioanalytical Chemistry*, *407*, 3285–3301.

Corso, G., Mäger, I., Lee, Yi., Görgens, A., Bultema, J., Giebel, B., Wood, M. J. A., Nordin, J. Z., & Andaloussi, S. E. (2017). Reproducible and scalable purification of extracellular vesicles using combined bind-elute and size exclusion chromatography. *Science Reports*, *7*, 11561.

Cushing, R. S., & Lawler, D. F. (1998). Depth filtration: Fundamental investigation through three-dimensional trajectory analysis. *Environmental Science & Technology*, *32*, 3793–3801.

Darby, J. L., Lawler, D. F., & Wilshusen, T. P. (1991). Depth filtration of wastewater: Particle size and ripening. *Research Journal of the Water Pollution Control Federation*, *63*, 228–238.

Datta, S., & Redner, S. (1998). Gradient clogging in depth filtration. *Physical Review A, Atomic, Molecular, and Optical Physics*, *58*(2), R1203–R1206.

Filant, J., Nejad, P., Paul, A., Simonson, B., Srinivasan, S., Zhang, X., Balaj, L., Das, S., Gandhi, R., Laurent, L. C., & Sood, A. K. (2018). Isolation of extracellular RNA from serum/plasma. *Methods in Molecular Biology*, *1740*, 43–57.

Garvey, W. T, Kwon, S., Zheng, D., Shaughnessy, S., Wallace, P., Hutto, A., Pugh, K., Jenkins, A. J., Klein, R. L., & Liao, Y. (2003). Effects of insulin resistance and type 2 diabetes on lipoprotein subclass particle size and concentration determined by nuclear magnetic resonance. *Diabetes*, *52*, 453–462.

Gemoll, T., Strohkamp, S., Rozanova, S., Röder, C., Hartwig, K., Kalthoff, H., Lehr, S., Elsharawy, A., & Habermann, J. (2020). Protein profiling of serum extracellular vesicles reveals qualitative and quantitative differences after differential ultracentrifugation and exoquicktm isolation. *Journal of Clinical Medicine*, *9*, 1429.

Ghaemi, N., Madaeni, S. S., Alizadeh, A., Daraei, P., Vatanpour, V., & Falsafi, M. (2012). Fabrication of cellulose acetate/sodium dodecyl sulfate nanofiltration membrane: Characterization and performance in rejection of pesticides. *Desalination*, *290*, 99–106.

Goldrick, S., Joseph, A., Mollet, M., Turner, R., Gruber, D., Farid, S. S., & Titchener-Hooker, N. J. (2017). Predicting performance of constant flow depth filtration using constant pressure filtration data. *Journal of Membrane Science*, *531*, 138–147.

Gonzales, P. A., Pisitkun, T., Hoffert, J. D., Tchapyjnikov, D., Star, R. A., Kleta, R., Wang, N. S., & Knepper, M A. (2009). Large-scale proteomics and phosphoproteomics of urinary exosomes. *Journal of the American Society of Nephrology*, *20*, 363–379.

Gonzalez-Begne, M., Lu, B., Han, X., Hagen, F. K., Hand, A. R., Melvin, J. E., & Yates, J. R. (2009). Proteomic analysis of human parotid gland exosomes by multidimensional protein identification technology (MudPIT). *Journal of Proteome Research*, *8*(3), 1304–1314.

Guo, S., Chen, J., Chen, F., Zeng, Q., Liu, W.-L., & Zhang, Ge. (2021). Exosomes derived from Fusobacterium nucleatum -infected colorectal cancer cells facilitate tumour metastasis by selectively carrying miR-1246/92b-3p/27a-3p and CXCL16. *Gut*, *70*, 1507–1519.

Haraszti, R. A., Miller, R., Stoppato, M., Sere, Y. Y., Coles, A., Didiot, M.-C., Wollacott, R., Sapp, E., Dubuke, M. L., Li, X., Shaffer, S. A., Difiglia, M., Wang, Y., Aronin, N., & Khvorova, A. (2018). Exosomes produced from 3D cultures of MSCs by tangential flow filtration show higher yield and improved activity. *Molecular Therapy*, *26*, 2838–2847.

He, L., Zhu, D., Wang, J., & Wu, X. (2019). A highly efficient method for isolating urinary exosomes. *International Journal of Molecular Medicine*, *43*(1), 83–90.

Höppener, J. W. M., Ahrén, B., & Lips, C. J. M. (2000). Islet amyloid and type 2 diabetes mellitus. *New England Journal of Medicine*, *343*, 411–419.

Johnsen, K. B., Gudbergsson, J. M., Andresen, T. L., & Simonsen, J. B. (2019). What is the blood concentration of extracellular vesicles? Implications for the use of extracellular vesicles as blood-borne biomarkers of cancer. *Biochimica et Biophysica Acta - Reviews on Cancer*, *1871*, 109–116. https://doi.org/10.1016/j.bbcan.2018.11.006

Jung, H. H., Kim, J.-Y., Lim, J. E., & Im, Y.-H. (2020). Cytokine profiling in serum-derived exosomes isolated by different methods. Science Reports. https://doi.org/10.1038/s41598-020-70584-z

Karimi, N., Cvjetkovic, A., Jang, S. C., Crescitelli, R., Hosseinpour Feizi, M. A., Nieuwland, R., Lötvall, J., & Lässer, C. (2018). Detailed analysis of the plasma extracellular vesicle proteome after separation from lipoproteins. *Cellular and Molecular Life Sciences*, *75*(15), 2873–2886. https://doi.org/10.1007/s00018-018-2773-4. Epub 2018 Feb 13. PMID: 29441425; PMCID: PMC6021463.

Keshelava, V., Zemskova, M., & Sorokin, K. (2019). Method and device for separating extracellular vesicles from biological liquids with the aid of cascade ultrafiltration, WO2019132688A1.

Khan, S. R., Glenton, P. A., Backov, R., & Talham, D. R. (2002). Presence of lipids in urine, crystals and stones: Implications for the formation of kidney stones. *Kidney International*, *62*, 2062–2072.

Khanal, O., Singh, N., Traylor, S. J., Xu, X., Ghose, S., Li, Z. J., & Lenhoff, A. M. (2018). Contributions of depth filter components to protein adsorption in bioprocessing. *Biotechnology Bioengineering*, *115*(8), 1938–1948.

Konoshenko, M. Y., Lekchnov, E. A., Vlassov, A. V., & Laktionov, P. P. (2018). Isolation of extracellular vesicles: General methodologies and latest trends. *BioMed Research International*, *8545347*, 1–27.

Kornilov, R., Puhka, M., Mannerström, B., Hiidenmaa, H., Peltoniemi, H., Siljander, P., Seppänen-Kaijansinkko, R., & Kaur, S. (2018). Efficient ultrafiltration-based protocol to deplete extracellular vesicles from fetal bovine serum. *Journal of Extracellular Vesicles*, *7*, 1422674.

Krafft, C., Wilhelm, K., Eremin, A., Nestel, S., Von Bubnoff, N., Schultze-Seemann, W., Popp, J., & Nazarenko, I. (2017). A specific spectral signature of serum and plasma-derived extracellular vesicles for cancer screening. *Nanomedicine: Nanotechnology, Biology and Medicine*, *13*(3), 835–841.

La Shu, S., Yang, Y., Allen, C. L., Hurley, E., Tung, K. H., Minderman, H., Wu, Y., & Ernstoff, M. S. (2020). Purity and yield of melanoma exosomes are dependent on isolation method. *Journal of Extracellular Vesicles*, *9*(1), 1692401.

Le Gall, L., Ouandaogo, Z. G., Anakor, E., Connolly, O., Butler Browne, G., Laine, J., Duddy, W., & Duguez, S. (2020). Optimized method for extraction of exosomes from human primary muscle cells. *Skeletal Muscle*, *10*(1), 20.

Liangsupree, T., Multia, E., & Riekkola, M.-L. (2021). Modern isolation and separation techniques for extracellular vesicles. *Journal of Chromatography A*, *1636*, 461773.

Lim, C. Z. J., Zhang, Y., Chen, Y., Zhao, H., Stephenson, M. C., Ho, N. R. Y., Chen, Y., Chung, J., Reilhac, A., Loh, T. P., Chen, C. L. H., & Shao, H. (2019). Subtyping of circulating exosome-bound amyloid β reflects brain plaque deposition. *Nature Communication*, *101*(10), 1–11.

Livshits, M. A., Khomyakova, E., Evtushenko, E. G., Lazarev, V. N., Kulemin, N. A., Semina, S. E., Generozov, E. V., & Govorun, V. M. (2015). Isolation of exosomes by differential centrifugation: Theoretical analysis of a commonly used protocol. *Science Reports*, *5*, 17319.

Lobb, R. J., Becker, M., Wen Wen, S., Wong, C. S. F., Wiegmans, A. P., Leimgruber, A., & Möller, A. (2015). Optimized exosome isolation protocol for cell culture supernatant and human plasma. *Journal of Extracellular Vesicles*, *4*, 27031.

Mahley, R. W., Innerarity, T. L., Rall, S. C., & Weisgraber, K. H. (1984). Plasma lipoproteins: Apolipoprotein structure and function. *Journal of Lipid Research*, *25*, 1277–1294.

Melo, S. A., Luecke, L. B., Kahlert, C., Fernandez, A. F., Gammon, S. T., Kaye, J., LeBleu, V. S., Mittendorf, E. A., Weitz, J., Rahbari, N., Reissfelder, C., Pilarsky, C., Fraga, M. F., Piwnica-Worms, D., & Kalluri, R. (2015). Glypican1 identifies cancer exosomes and facilitates early detection of cancer HHS Public Access. *Nature*, *523*(7559), 177–182.

Merchant, M. L., Powell, D. W., Wilkey, D. W., Cummins, T. D., Deegens, J. K., Rood, I. M., Mcafee, K. J., Fleischer, C., Klein, E., & Klein, J. B. (2010). Microfiltration isolation of human urinary exosomes for characterization by MS. *Proteomics—Clinical Applications*, *4*(1), 84–96.

Mikl, C., Peters, J., Trapp, M., Kornmueller, K., Schneider, W. J., & Prassl, R. (2011). Softness of atherogenic lipoproteins: A comparison of very low density lipoprotein (VLDL) and low density lipoprotein (LDL) using elastic incoherent neutron scattering (EINS). *Journal of the American Chemical Society*, *133*, 13213.

Mitaki, S., Wada, Y., Sheikh, A. M., Yamaguchi, S., & Nagai, A. (2021). Proteomic analysis of extracellular vesicles enriched serum associated with future ischemic stroke. *Science Reports*, *11*, 24024.

Momen-Heravi, F. (2017). Isolation of extracellular vesicles by ultracentrifugation. *Extracellular Vesicles*, *1660*, 25–32.

Narhi, L. O., Schmit, J., Bechtold-Peters, K., & Sharma, D. (2012). Classification of protein aggregates. *Journal of Pharmaceutical Sciences*, *101*, 493–498.

Nordin, J. Z., Lee, Y., Vader, P., Mäger, I., Johansson, H. J., Heusermann, W., Wiklander, O. P. B., Hällbrink, M., Seow, Y., Bultema, J. J., Gilthorpe, J., Davies, T., Fairchild, P. J., Gabrielsson, S., Meisner-Kober, N. C., Lehtiö, J., Smith, C. I. E., Wood, M. J. A., & Andaloussi, S. E. (2015). Ultrafiltration with size-exclusion liquid chromatography for high yield isolation of extracellular vesicles preserving intact biophysical and functional properties. *Nanomedicine: Nanotechnology, Biology and Medicine*, *11*(4), 879–883.

Ochieng, J., Pratap, S., Khatua, A. K., & Sakwe, A. M. (2009). Anchorage-independent growth of breast carcinoma cells is mediated by serum exosomes. *Experimental Cell Research*, *315*, 1875–1888.

Onur, A., Ng, A., Garnier, G., & Batchelor, W. (2018). Engineering cellulose fibre inorganic composites for depth filtration and adsorption. *Separation and Purification Technology*, *203*, 209–216.

Petersen, K. E., Shiri, F., White, T., Bardi, G. T., Sant, H., Gale, B. K., & Hood, J. L. (2018). Exosome isolation: Cyclical electrical field flow fractionation in low-ionic-strength fluids. *Analytical Chemistry*, *90*(21), 12783–12790.

Pienimaeki-Roemer, A., Kuhlmann, K., Böttcher, A., Konovalova, T., Black, A., Orsó, E., Liebisch, G., Ahrens, M., Eisenacher, M., Meyer, H. E., & Schmitz, G. (2015). Lipidomic and proteomic characterization of platelet extracellular vesicle subfractions from senescent platelets. *Transfusion*, *55*, 507–521.

Principe, S., Jones, E. E., Kim, Y., Sinha, A., Nyalwidhe, J. O., Brooks, J., Semmes, O. J., Troyer, D. A., Lance, R. S., Kislinger, T., & Drake, R R. (2013). In-depth proteomic analyses of exosomes isolated from expressed prostatic secretions in urine. *Proteomics*, *13*, 1667–1671.

Reinhardt, T. A., Lippolis, J. D., Nonnecke, B. J., & Sacco, R. E. (2012). Bovine milk exosome proteome. *Journal of Proteomics*, *75*, 1486–1492.

Rekker, K., Saare, M., Roost, A. M., Kubo, A.-L., Zarovni, N., Chiesi, A., Salumets, A., & Peters, M. (2014). Comparison of serum exosome isolation methods for microRNA profiling. *Clinical Biochemistry*, *47*, 135–138.

Ronquist, K. G., Ek, B., Morrell, J., Stavreus-Evers, A., Ström Holst, B., Humblot, P., Ronquist, G., & Larsson, A. (2013). Prostasomes from four different species are able to produce extracellular adenosine triphosphate (ATP). *Biochimica et Biophysica Acta (BBA) - General Subjects*, *1830*, 4604–4610.

Salehi, E., Askari, M., Aliee, M. H., Goodarzi, M., & Mohammadi, M. (2019). Data-based modeling and optimization of a hybrid column-adsorption/depth-filtration process using a combined intelligent approach. *Journal of Cleaner Production*, *236*, 117664.

Samuel, M., Chisanga, D., Liem, M., Keerthikumar, S., Anand, S., Ang, C.-S., Adda, C. G., Versteegen, E., Jois, M., & Mathivanan, S. (2017). Bovine milk-derived exosomes from colostrum are enriched with proteins implicated in immune response and growth. Science Reports, *7*.

Serrano-Pertierra, E., Oliveira-Rodríguez, M., Rivas, M., Oliva, P., Villafani, J., Navarro, A., Blanco-López, M., & Cernuda-Morollón, E. (2019). Characterization of plasma-derived extracellular vesicles isolated by different methods: A comparison study. *Bioengineering*, *6*(1), 8.

Shin, J.-B., Krey, J. F., Hassan, A., Metlagel, Z., Tauscher, A. N., Pagana, J. M., Sherman, N. E., Jeffery, E. D., Spinelli, K. J., Zhao, H., Wilmarth, P. A., Choi, D., David, L. L., Auer, M., & Barr-Gillespie, P. G. (2013). Molecular architecture of the chick vestibular hair bundle. *Nature Neuroscience*, *163*(16), 365–374.

Shtam, T. A., Samsonov, R. B., Volnitskiy, A. V., Kamyshinsky, R. A., Verlov, N. A., Kniazeva, M. S., Korobkina, E. A., Orehov, A. S., Vasiliev, A. L., Konevega, A. L., & Malek, A. V. (2018). Isolation of extracellular microvesicles from cell culture medium: Comparative evaluation of methods. *Biochemistry (Moscow) Supplement Series B Biomedical Chemistry*, *12*(2), 167–175.

Sidhom, K., Obi, P. O., & Saleem, A. (2020). A review of exosomal isolation methods: Is size exclusion chromatography the best option? *International Journal of Molecular Sciences*, *21*(18), 6466.

Skliar, M., Chernyshev, V. S., Belnap, D. M., Sergey, G. V., Al-Hakami, S. M., Bernard, P. S., Stijleman, I. J., & Rachamadugu, R. (2018). Membrane proteins significantly restrict exosome mobility. *Biochemical and Biophysical Research Communications*, *501*, 1055–1059.

Slyusarenko, M., Nikiforova, N., Sidina, E., Nazarova, I., Egorov, V., Garmay, Y., Merdalimova, A., Yevlampieva, N., Gorin, D., & Malek, A. (2021). Formation and evaluation of a two-phase polymer system in human plasma as a method for extracellular nanovesicle isolation. *Polymers (Basel)*, *13*(3), 458.

Soares Martins, T., Catita, J., Martins Rosa, I., A B Da Cruz E Silva, O., & Henriques, A. G. (2018). Exosome isolation from distinct biofluids using precipitation and column-based approaches. *PLoS One*, *13*(6), e0198820.

Sódar, B. W., Kittel, Á., Pálóczi, K., Vukman, K. V., Osteikoetxea, X., Szabó-Taylor, K., Németh, A., Sperlágh, B., Baranyai, T., Giricz, Z., Wiener, Z., Turiák, L., Drahos, L., Pállinger, É., Vékey, K., Ferdinandy, P., Falus, A., & Buzás, E. I. (2016). Low-density lipoprotein mimics blood plasma-derived exosomes and microvesicles during isolation and detection. *Science Reports*, *6*, 24316.

Sossna, M., Hollas, M., Schaper, J., & Scheper, T. (2007). Structural development of asymmetric cellulose acetate microfiltration membranes prepared by a single-layer dry-casting method. *Journal of Membrane Science*, *289*, 7–14.

Stamer, W. D., Hoffman, E. A., Luther, J. M., Hachey, D. L., & Schey, K. L. (2011). Protein profile of exosomes from trabecular meshwork cells. *Journal of Proteomics*, *74*, 796–804.

Suárez, H., Andreu, Z., Mazzeo, C., Toribio, V., Pérez-Rivera, A. E., López-Martín, S., García-Silva, S., Hurtado, B., Morato, E., Peláez, L., Arribas, E. A., Tolentino-Cortez, T., Barreda-Gómez, G., Marina, A. I., Peinado, H., & Yáñez-Mó, M. (2021). CD9 inhibition reveals a functional connection of extracellular vesicle secretion with mitophagy in melanoma cells. *Journal of Extracellular Vesicles*, *10*(7), e12082.

Sun, Y., Saito, K., & Saito, Y. (2019). Lipid profile characterization and lipoprotein comparison of extracellular vesicles from human plasma and serum. *Metabolites*, *9*, 259.

Sutherland, K. (2008). *Filters and filtration handbook* (2nd ed.). Elsevier.

Syková, E., & Nicholson, C. (2008). Diffusion in brain extracellular space. *Physiological Reviews*, *88*, 1277–1340.

Tamm, I., & Horsfall, F. L. (1950). Characterization and separation of an inhibitor of viral hemagglutination present in urine. *Experimental Biology and Medicine*, *74*, 108–114.

Tauro, B. J., Greening, D. W., Mathias, R. A., Ji, H., Mathivanan, S., Scott, A. M., & Simpson, R. J. (2012). Comparison of ultracentrifugation, density gradient separation, and immunoaffinity capture methods for isolating human colon cancer cell line LIM1863-derived exosomes. *Methods (San Diego, California)*, *56*, 293–304.

Taylor, D. D., & Shah, S. (2015). Methods of isolating extracellular vesicles impact down-stream analyses of their cargoes. *Methods (San Diego, California)*, *87*, 3–10.

Théry, C., Amigorena, S., Raposo, G., & Clayton, A. (2006). Isolation and characterization of exosomes from cell culture supernatants and biological fluids. Current Protocols in Cell Biology.

Tutanov, O., Orlova, E., Proskura, K., Grigor'eva, A., Yunusova, N., Tsentalovich, Y., Alexandrova, A., & Tamkovich, S. (2020). Proteomic analysis of blood exosomes from healthy females and breast cancer patients reveals an association between different exosomal bioactivity on non-tumorigenic epithelial cell and breast cancer cell migration in vitro. *Biomolecules*, *10*, 495.

Van Niel, G., Raposo, G., Candalh, C., Boussac, M., Hershberg, R., Cerf–Bensussan, N., & Heyman, M. (2001). Intestinal epithelial cells secrete exosome-like vesicles. *Gastroenterology*, *121*, 337–349.

Van Reis, R., Gadam, S., Frautschy, L. N., Orlando, S., Goodrich, E. M., Saksena, S., Kuriyel, R., Simpson, C. M., Pearl, S., & Zydney, A. L. (1997). High performance tangential flow filtration. *Biotechnology and Bioengineering*, *56*, 71–82.

Vázquez-Oliva, G., Zamora, A., Ramos, R., Subirana, I., Grau, M., Dégano, I R., Muñoz, D., Fitó, M., Elosua, R., & Marrugat, J. (2018). Analysis of plasma albumin, vitamin D, and apolipoproteins A and B as predictive coronary risk biomarkers in the REGICOR study. *Revista Española de Cardiología (English Edition)*, *71*, 910–916.

Walker, J. M. (2009). *Influenza virus methods and protocols*. Humana Press.

Webber, J., & Clayton, A. (2013). How pure are your vesicles? *Journal of Extracellular Vesicles*, *2*, 19861.

Welton, J. L., Webber, J. P., Botos, L.-A., Jones, M., & Clayton, A. (2015). Ready-made chromatography columns for extracellular vesicle isolation from plasma. *Journal of Extracellular Vesicles*, *4*, 27269.

Wiśniewski, J. R., Zougman, A., Nagaraj, N., & Mann, M. (2009). Universal sample preparation method for proteome analysis. *Nature Methods*, *6*(5), 359–362.

Witwer, K. W., Buzás, E. I., Bemis, L. T., Bora, A., Lässer, C., Lötvall, J., Nolte-'T Hoen, E. N., Piper, M. G., Sivaraman, S., Skog, J., Théry, C., Wauben, M. H., & Hochberg, F. (2013). Standardization of sample collection, isolation and analysis methods in extracellular vesicle research. *Journal of Extracellular Vesicles*, *2*, 1–25.

Yamada, T., Inoshima, Y., Matsuda, T., & Ishiguro, N. (2012). Comparison of methods for isolating exosomes from bovine milk. *Journal of Veterinary Medical Science*, *74*(11), 1523–1525.

Yang, Y., Wang, Y., Wei, S., Zhou, C., Yu, J., Wang, G., Wang, W., & Zhao, L. (2021). Extracellular vesicles isolated by size-exclusion chromatography present suitability for RNomics analysis in plasma. *Journal of Translational Medicine*, *19*, 104.

Zhang, X., Borg, E. G. F., Liaci, A. M, Vos, H. R., & Stoorvogel, W. (2020). A novel three step protocol to isolate extracellular vesicles from plasma or cell culture medium with both high yield and purity. *Journal of Extracellular Vesicles*, *9*, 1791450, https://doi.org/10.1080/20013078.2020.1791450

Zhdanova, D. Y., Poltavtseva, R. A., Svirshchevskaya, E. V., & Bobkova, N. V. (2021). Effect of intranasal administration of multipotent mesenchymal stromal cell exosomes on memory of mice in alzheimer's disease model. *Bulletin of Experimental Biology and Medicine*, *170*(3), 575–582.

SUPPORTING INFORMATION

Additional supporting information can be found online in the Supporting Information section at the end of this article.